bioRxiv preprint doi: https://doi.org/10.1101/394403; this version posted August 26, 2018. The copyright holder for this preprint (which was not certified by peer review) is the author/funder, who has granted bioRxiv a license to display the preprint in perpetuity. It is made available under aCC-BY-NC 4.0 International license.

Neural circuit basis of aversive odour processing in *Drosophila* from sensory input to descending output

Paavo Huoviala[1,2] , Michael-John Dolan[1,3,5], Fiona M. Love[2,5], Shahar Frechter[1], Ruairí J.V. Roberts[2], Zane Mitrevica[2], Philipp Schlegel[2] , Alexander Shakeel Bates[1], Yoshinori Aso[3], Tiago Rodrigues[1], Hannah Cornwall[1], Marcus Stensmyr[4], Davi Bock[3], Gerald M. Rubin[3], Marta Costa[2], Gregory S.X.E. Jefferis[1,2]

[1]Division of Neurobiology, MRC Laboratory of Molecular Biology, Cambridge CB2 0QH, UK
[2]Department of Zoology, University of Cambridge, CB2 3EJ, UK
[3]Janelia Research Campus, Howard Hughes Medical Institute, United States
[4]Department of Biology, Lund University, 22100 Lund, Sweden
[5]Equal Contributions
Contact: jefferis@mrc-lmb.cam.ac.uk

https://doi.org/10.1101/394403

Abstract

Evolution has tuned the nervous system of most animals to produce stereotyped behavioural responses to ethologically relevant stimuli. For example, female *Drosophila* avoid laying eggs in the presence of geosmin, an odorant produced by toxic moulds. Using this system, we now identify third order olfactory neurons that are essential for an innate aversive behaviour. Connectomics data place these neurons in the context of a complete synaptic circuit from sensory input to descending output. We find multiple levels of valence-specific convergence, including a novel form of axo-axonic input onto second order neurons conveying another danger signal, the pheromone of parasitoid wasps. However we also observe a massive divergence as geosmin-responsive second order olfactory neurons connect with a diverse array of ~75 cell types. Our data suggest a transition from a labelled line organisation in the periphery to one in which olfactory information is mapped onto many different higher order populations with distinct behavioural significance.

Keywords: Neural circuits, Innate Behaviour, Olfaction, Valence, Connectomics

Introduction

Studying the neural circuit basis of innate behaviours in simple model organisms provides an ideal platform to discover how sensory signals are transformed into behavioural responses by the nervous system, arguably one of the fundamental goals of neuroscience. The olfactory system is a particularly shallow sensory modality where the sensory periphery is only two synapses away from higher brain areas important for organising behaviour and forming memories. In both insects and mammals, after processing in the first olfactory centre, divergent projections relay information to different higher olfactory centres, some of which appear to be specialised for innate behaviour and others for learning and memory [1–4].

The periphery of the *Drosophila* olfactory system consists of ~1300 sensory neurons (ORNs) of ~50 distinct types, on each side [5,6]. Each type, with a few exceptions, expresses only a single olfactory receptor that determines the neurons' response profile and characteristics [6–8]. Many receptors are quite broadly tuned, and for this reason, odours are typically encoded in the combinatorial activity of this parallel array of odour channels. However in certain cases of odours of particular ethological relevance may be encoded in the activity of just one odour channel. This situation of functionally segregated pathways, is sometimes referred to as labelled line encoding [9–12]. The ORNs send their axons into the antennal lobe (AL) in the brain, where the ORNs expressing the same receptor converge onto just 1-10, presumably identical, second order projection neurons (PNs) and local neurons in ~50 distinct glomeruli [13,14]. From the AL the axons of the PNs then go on to project to two higher olfactory processing centres: the mushroom body (MB) and the lateral horn (LH).

The MB is crucial for associative learning, and key advances have been made in recent years regarding its circuit architecture and function, and the writing and retrieval of memories of different valence [15–18]. However, our understanding of the LH remains considerably more limited. The LH is thought to be important for innate odour responses [19], the PN axonal arbours in the LH have been shown to be hard-wired and stereotyped across animals, and the general architecture of the brain area has been proposed to be organised by behavioural relevance of the afferent odour channels [20], thus demonstrating some kind of behaviourally defined topography. However, to date, no direct evidence for the role of lateral horn neurons (LHNs) in innate odour-guided behaviours has been published. Furthermore, only the pheromonal cVA-processing circuit has been traced until third order neurons of the lateral horn [21–23].

The study of labelled line encoding potentially has significant experimental advantages for linking olfactory circuits to behaviour. Indeed an ideal approach would be to trace labelled line odour channels of varying and well understood behavioural significance to the LH in order to test if LHNs are required for innate odour-guided behaviours, and also sufficient to trigger them when activated. Such an approach might also reveal if the general organisation of the LH is indeed defined by behavioural relevance, so that odour channels containing information of similar meaning to the animal synapse onto the same LHNs, the activity of which would then trigger an appropriate behavioural response. A specific opportunity to achieve this is offered by studying

bioRxiv preprint doi: https://doi.org/10.1101/394403; this version posted August 26, 2018. The copyright holder for this preprint (which was not certified by peer review) is the author/funder, who has granted bioRxiv a license to display the preprint in perpetuity. It is made available under aCC-BY-NC 4.0 International license.

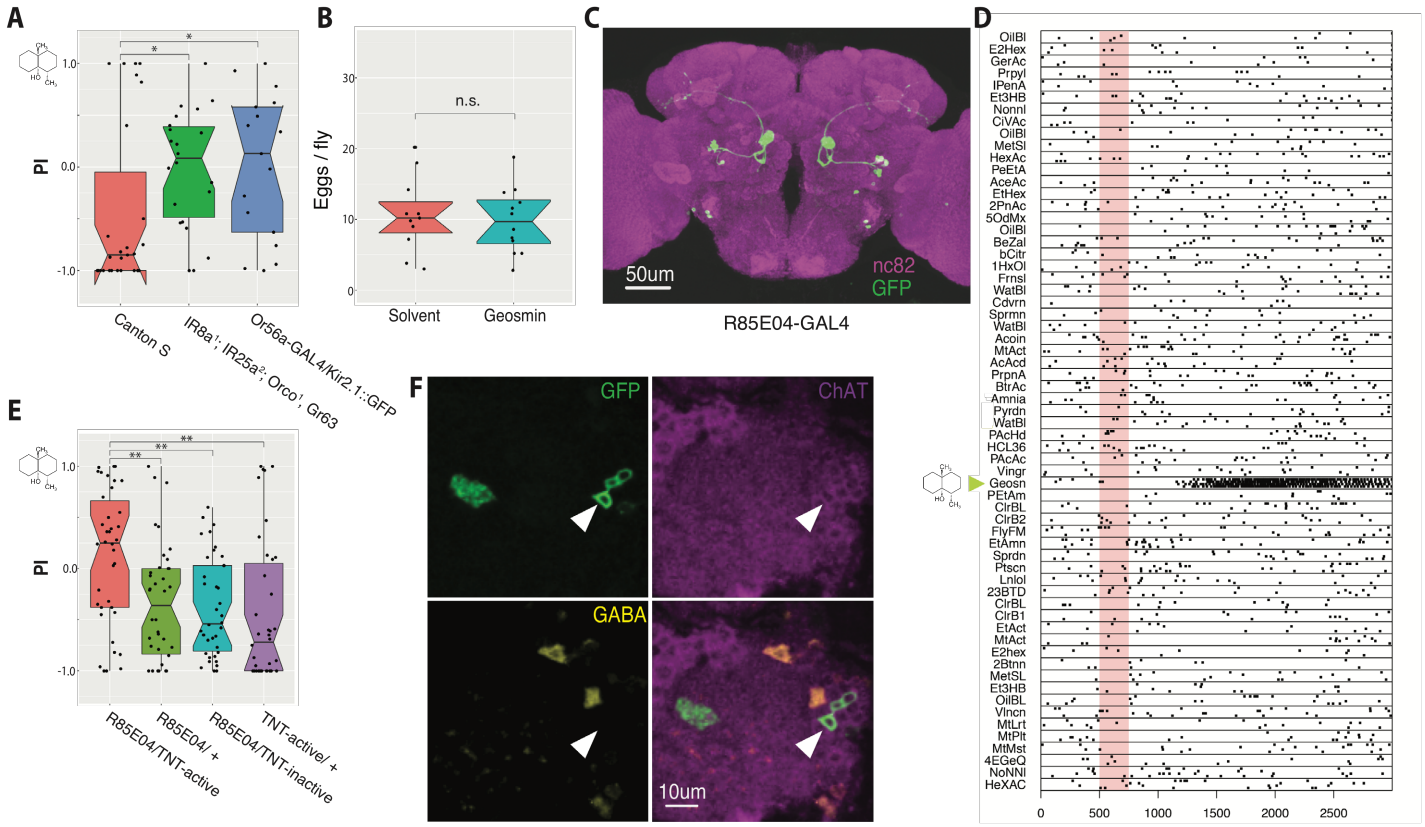

Figure 1: DA2 PNs labelled by R85E04-GAL4 are excitatory PNs that respond to geosmin and are required for geosmin avoidance behaviour.
(A) Egg-laying two-choice preference indices (PI) to geosmin for wild type (Canton S) flies, anosmic mutants, and flies with silenced geosmin responsive sensory neurons (Or56a ORNs). The chemical structure for geosmin marks the stimulus side. Groups are compared by a Kruskal-Wallis rank sum test followed by planned comparisons of wild type group to the other groups by Wilcoxon rank sum tests with Holm-Bonferroni corrections. n=27 (left), n=22 (middle), and n=17 (right).
(B) Eggs laid per wild type fly under geosmin or solvent exposure (Welch's Two Sample t-test. n=12, n=11).
(C) Expression pattern of R85E04, a GAL4 line that labels 5-6 DA2 PNs. A JFRC2 registered maximum intensity projection of a female brain, raw image data from Flylight database (http://flweb.janelia.org/cgi-bin/flew.cgi) [28]. Green channel is GFP and magenta, nc82 neuropil stain.
(D) Raster plot of in vivo patch clamp recordings from DA2 PNs (R85E04-GAL4) to a panel of odorants [44]. Odour valve opening denoted by pale red bar, timebase ms.
(E) Egg-laying two-choice preference indices (PI) to geosmin while silencing putative geosmin sensing PNs by expressing tetanus toxin light-chain (TNT) [30] via R85E04 (groups compared by a Kruskal-Wallis rank sum test followed by post-hoc comparisons of experimental group to each of the parental groups by Wilcoxon rank sum tests with Holm-Bonferroni corrections. n=38 for all groups).
(F) Immunostainings against GFP, ChAT, and GABA in R85E04-GAL4, and the merge of the three. Single slices of confocal stacks showing the AL (magenta counterstain) and PN cell bodies (arrowheads). Significance values: * $p<0.05$ ** $p<0.01$

olfactory processing of the innately aversive compound geosmin [12]. Geosmin is a microbe-produced, aversion triggering, volatile chemical detected by a dedicated receptor, Or56a, expressed by only a single class of sensory neurons housed in the ab4 sensilla of the fly antennae [12]. The clearly defined behavioural significance of this signal, together with Or56a-expressing sensory neurons being the sole, dedicated geosmin sensors of the animal, make this functionally segregated pathway an ideal target for studies on how smells are transformed into behavioural responses in the fly brain.

Here we use a combination of light and electron microscopy-based neuroanatomy, behavioural assays, electrophysiology, and functional imaging to trace the geosmin processing circuit from the periphery to the third order LHNs and select fourth order descending interneurons. We identify behaviourally necessary second order neurons, and necessary and sufficient third order neurons. We find convergence of multiple aversive odour channels in the LH: DA2 PNs form axo-axonic synapses onto the aversive DL4 PNs, and some LHNs receive inputs from several aversive PNs. However, we also find substantial divergence of the DA2 PN channel onto multiple LHN targets. Taken together the data show that while the path from sensory inputs to motor outputs may be as shallow as previously suggested (a minimum of 3 synapses between periphery and the nerve cord [22]), even for a labelled line encoded stimulus the circuit broadens massively at the transition from second to third order level. This organisation might reflect the demands of more complex higher-order computations, needed by the animal to select a suitable behavioural response to a given sensory stimulus in a variable environment.

Results

Geosmin causes aversion in an egg-laying context but does not inhibit egg-laying, or affect other sexually dimorphic behaviours

Stensmyr *et al.* [12] showed that flies strongly avoid geosmin in an egg-laying context using a two-choice oviposition assay. Additionally, flies

bioRxiv preprint doi: https://doi.org/10.1101/394403; this version posted August 26, 2018. The copyright holder for this preprint (which was not certified by peer review) is the author/funder, who has granted bioRxiv a license to display the preprint in perpetuity. It is made available under aCC-BY-NC 4.0 International license.

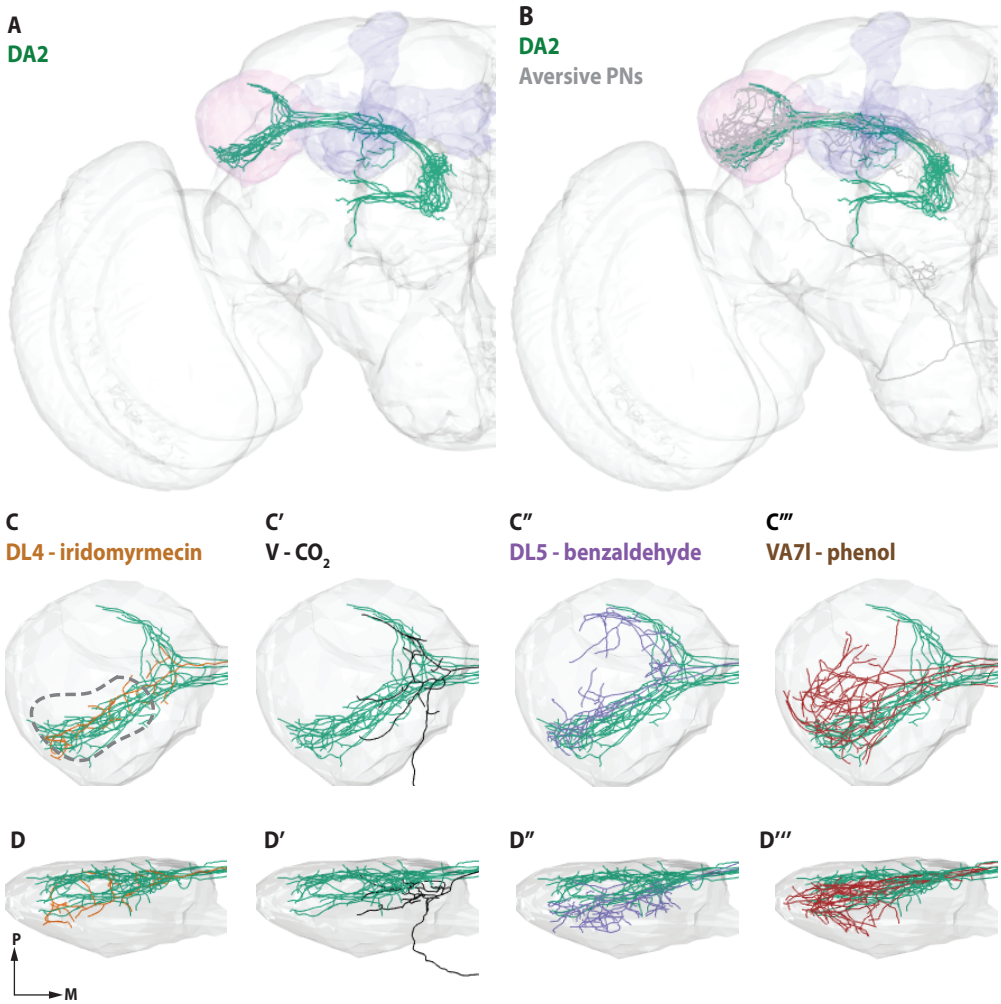

Figure 2: DA2 PN axons are morphologically similar to other aversive PNs in the LH.
(A) Frontal view of DA2 PNs traced from confocal image stacks (n=8). MB is shown in light blue and LH in light magenta, for reference. Neurons are from multiple brains.
(B) Frontal view of DA2 PNs (green, same as A) together with selected aversive PNs (DL4, V, DL5, VA7l, all in grey).
(C-C‴) Frontal view of DA2 PN axons (green) with other known aversive PNs in the LH. Known ligands are shown for each odour channel. Dashed line marks a putative zone of aversive convergence.
(D-D‴) Dorsal view of DA2 PN axons (green) with other aversive PNs in the LH.
Tracings for DL5 (n=2) and VA7l (n=4) from [20]. DA2 (n=8), DL4 (n=1), and V (n=1) traced from FCWB registered [32] confocal images from the FlyCircuit image dataset [31].

showed a milder avoidance in feeding and T-maze assays, as well as a minor reduction in walking speed in the Flywalk assay [12,24] in response to the odour. Given the stronger results in the egg-laying context and the ethological rationale of geosmin as a signal for the presence of microorganisms that prevent development of *Drosophila* eggs, we selected the egg-laying two-choice assay as the primary behavioural basis for further experiments.

As shown by earlier work [12], wild-type flies avoid geosmin in an egg-laying two-choice assay, and this avoidance is solely due to olfaction, more specifically, the Or56a expressing sensory neurons (**fig 1A, fig S1A**). As geosmin quantity did not appear to have a significant effect on the magnitude of the behavioural phenotype (**fig S1B**), we opted for the smaller (5ul of 1:1000 dilution of geosmin) of the tested quantities for the rest of our experiments. Using yeast as an olfactory stimulus resulted in robust attraction (**fig S1C**), showing that we can see both aversion and attraction by using the same behavioural assay. As the egg-laying aversion could in principle result from either positional aversion to the odorant, or by geosmin directly decreasing egg-laying, we also tested if geosmin affects egg-laying quantity in a no-choice situation. However, this appeared not to be the case: even high stimulus quantities (50 ul of 1:1000 dilution of geosmin) had no effect on the number of eggs-laid (**fig 1B**). On the other hand, geosmin caused no discernable avoidance in a trap-assay when given the choice between just yeast or yeast and geosmin, neither in virgin nor mated females (although we did observe more mated females entering both traps, potentially due to an increased attraction to yeast odour) (**fig S1D-E**), further suggesting that its aversive effect might be particularly strong in the context of a search for a suitable egg-laying site. A related recent example of the behavioural state of the animal affecting the valence of an olfactory stimulus is given by a recent study [25] that shows that CO_2, a commonly used aversive cue, can actually be attractive for foraging flies. Finally, we wanted to test whether geosmin affects any other reproduction related fly behaviours. However, we found no effect on male courtship, or female receptivity (**fig S1F-I**).

DA2 projection neurons are necessary for geosmin avoidance

Or56a expressing ORNs project to the DA2 glomerulus of the antennal lobe (AL) where they synapse with PNs that project to higher olfactory processing centers. Stensmyr *et al.* [12] performed patch clamp recordings from 66 PNs from 31 different glomeruli and found just two geosmin responsive neurons, and the dendrites of both targeted the DA2 glomerulus. This suggests that at the level of second order neurons, geosmin information is still represented as a labelled line code, similar to how pheromones are processed in the insect brain [26,27].

We wanted a way to reproducibly target the geosmin responsive DA2 PNs in order to manipulate and record the activity of these neurons. To this end, we visually screened the FlyLight collection (http://flweb.janelia.org/cgi-bin/flew.cgi) [28] for GAL4 driver lines showing expression in the PNs. An initial search returned a driver line (R85E04) selectively labeling 5-6 uniglomerular PNs per hemisphere, which appeared to target the DA2 glomerulus, along with 3-4 neurons

bioRxiv preprint doi: https://doi.org/10.1101/394403; this version posted August 26, 2018. The copyright holder for this preprint (which was not certified by peer review) is the author/funder, who has granted bioRxiv a license to display the preprint in perpetuity. It is made available under aCC-BY-NC 4.0 International license.

in the antennal mechanosensory and motor centre (**fig 1C**) and 1-2 neurons in the ventral nerve cord (not shown). To anatomically verify that the PNs labelled by R85E04 are indeed DA2 PNs, and postsynaptic to the geosmin sensing Or56a-expressing neurons, we expressed a genetically encoded chemical Halo-tag [29] in both the sensory neurons and the PNs by using a combination of Or56a-GAL4 and R85E04 driver lines, confirming that the expression in the ORNs and PNs was restricted to the same glomerulus (**fig S1J**). Like other PNs taking the same medial antennal lobe tract, the DA2 PNs were positively labelled by anti-choline acetyltransferase antibody (ChAT), but not anti-GABA, and are thus excitatory (**fig 1F**).

Next, in order to confirm that geosmin information is indeed passed to R85E04 DA2 PNs, we carried out *in vivo* whole-cell patch clamp recordings. These revealed strong and highly selective responses to geosmin (**fig 1D**), again supporting the labelled line coding of geosmin. We then proceeded to test the flies' behavioural response to geosmin with the egg-laying two-choice assay while silencing the synaptic output of DA2 PNs by expressing the tetanus toxin light-chain [30] via R85E04. This resulted in a striking abolishment of the avoidance behaviour (**fig 1E**). The behavioural phenotype was indistinguishable from anosmic flies (**fig 1A**), suggesting that the DA2 PNs are absolutely necessary for geosmin sensing. In summary, R85E04 labels excitatory PNs postsynaptic to Or56a-expressing ORNs, that respond strongly and selectively to geosmin, and are necessary for geosmin avoidance behaviour in the context of egg-laying, an ecologically highly relevant task for the animal.

Aversive PNs are morphologically similar to each other and target the same region of the LH

We next wanted to look at DA2 PN axonal morphology in more detail to look for potential downstream targets in the geosmin processing circuit. To do this, we digitally reconstructed the 3D morphology of the neurons from available registered confocal image data of stochastically labelled single neurons of the FlyCircuit dataset [31,32] (**fig 2A**). DA2 PNs project exclusively to the LH and mushroom body (MB) calyx. In the absence of stereotyped connectivity at the PN-MB Kenyon cell (KC) synapses [15], we thought it unlikely that MB connections mediate behavioural responses to an innately aversive odor like

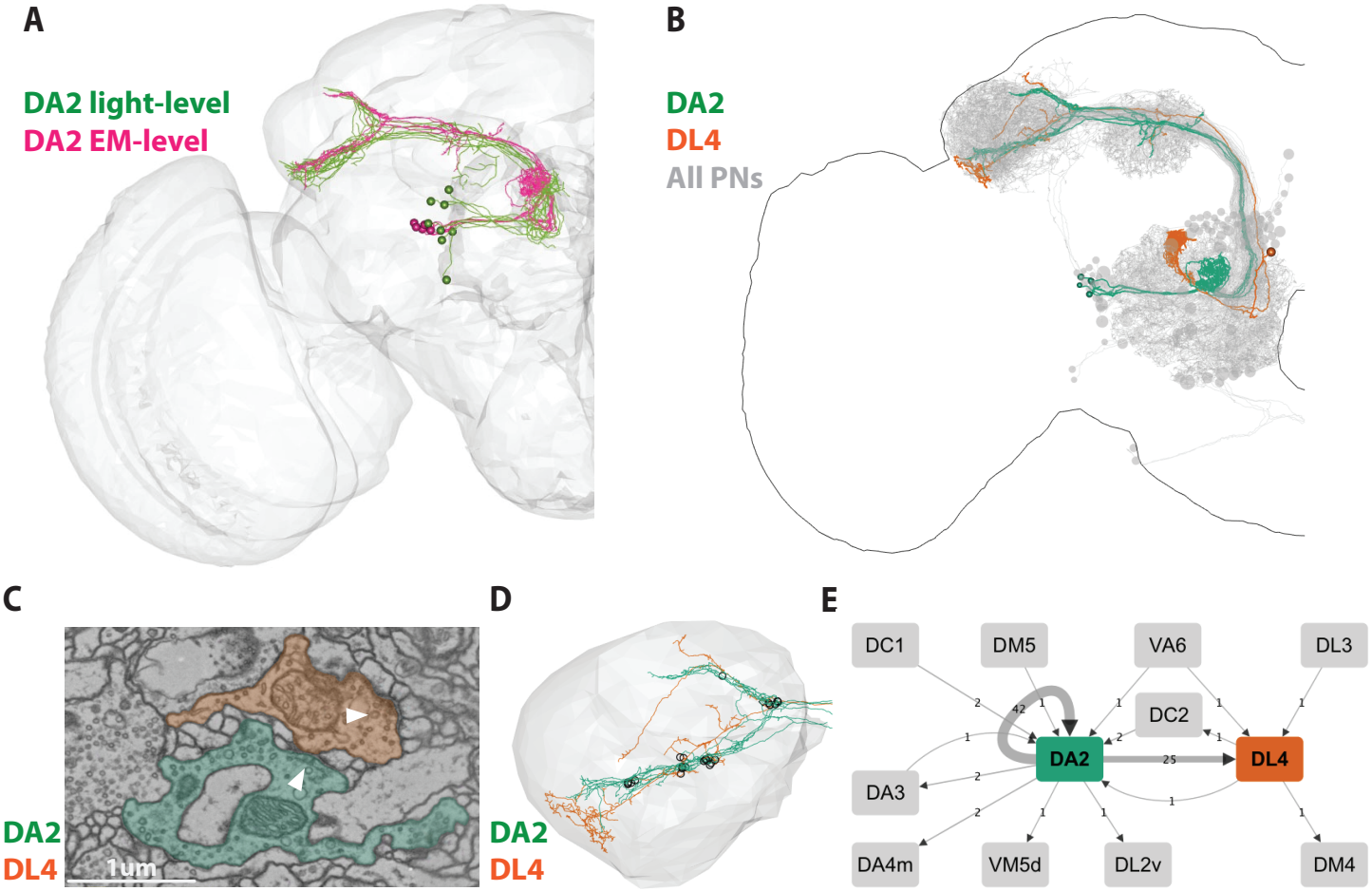

Figure 3: Axo-axonic convergence of DA2 and DL4 PN channels.
(A) Frontal view of light (green) and EM-level (magenta) tracings of DA2 PNs (n=5 for EM, and same as fig 2A for light level tracings). The EM-level tracings are transformed into the FCWB reference space via bridging registrations.
(B) Frontal view of EM-level reconstructions of DA2 (green, same as A) and DL4 (orange) PNs together with all excitatory uniglomerular PNs (used for identifying DA2 and DL4 PNs) traced in the dataset, shown in the FAFB reference brain.
(C) An example EM image showing one DA2 PN (green) to DL4 (orange) PN axo-axonic synapse in the LH. The arrowheads mark the presynaptic sites.
(D) Location of axo-axonic synapses from DA2 PNs to the DL4 PN in the LH (grey) (open circles), and vice versa (open square).
(E) A connectivity graph of axo-axonic uniglomerular PN synapses to and from DA2 PNs (n=5) on the right side of the brain.

bioRxiv preprint doi: https://doi.org/10.1101/394403; this version posted August 26, 2018. The copyright holder for this preprint (which was not certified by peer review) is the author/funder, who has granted bioRxiv a license to display the preprint in perpetuity. It is made available under aCC-BY-NC 4.0 International license.

geosmin. Nevertheless, to test this possibility, we silenced KC synaptic output by driving the expression of tetanus toxin via a broad MB driver line MB247-GAL4. The results confirmed that MB KCs are not required for geosmin avoidance (**fig S1K**), so we focussed our attention on the LH arbours.

Several classes of PNs implicated in aversive odour processing [12,33–36] appear to have very similar axonal arborisations in the LH (**fig 2B-D'''**). While some of the aversive PNs—like the DA2 and the bilateral CO_2 sensing V PNs—form crescent shaped arborisations, projecting both to ventral and dorsal parts of the LH [37], all of the PNs shown here appear to have projections in the ventral-posterior LH (dashed line in **fig 2C**). As has recently been pointed out [33], the DL4 PNs in particular have very similar axonal arborisations to those of the DA2 PNs in this part of the LH (**fig 2C**). DL4 PNs are postsynaptic to the parasitic wasp *Leptopilina boulardi* pheromone (consisting of iridomyrmecin, actinidine, and nepatalactol) sensing Or49a/Or85f ORNs. This observation is especially interesting as the authors showed that wasp odour is aversive in an egg-laying context, but not in T-maze or trap-assays [33]. The morphological data, taken together with a recent study where the authors artificially activated different ORN channels in an egg-laying context [38] and saw that many of the most aversive odour channels project to the ventral-posterior LH, suggests that this region might be of special significance for egg-laying aversion, and hints at the possibility of valence-based integration of multiple odour channels taking place in the LH.

EM connectomics reveals axo-axonic convergence of aversive PNs and extensive divergence of the DA2 pathway in the LH

In order to look for downstream targets of the geosmin processing circuit, and thus also LH neurons that might act as integrators based on the behavioural valence of the odours, we took two parallel approaches. First, we reconstructed DA2 PNs and their postsynaptic 3rd order partners in the LH in a recently acquired whole-brain electron-microscopy (EM) volume of the female *Drosophila [39]* using the CATMAID software toolkit [40,41]. Secondly, we performed a light-level anatomical *in silico* screen to look for genetic driver lines containing LHNs putatively downstream of DA2 PNs. These approaches complement each other: EM tracing, while much more laborious, provides unambiguous confirmation of synaptic connectivity between DA2 PNs and their partner neurons; light-level screening provides a faster route to obtain reagents for behavioural or functional connectivity testing. We will discuss the EM connectomics approach first, followed by the light-level screen.

Zheng *et al.* [39] had recently identified 5 DA2 PNs on the right-hand side of the whole-brain EM volume. We carefully verified this identification, independently identified the glomerulus on the left hand side of the fly brain, and showed that these two glomeruli are co-innervated by the same ORNs (like most *Drosophila* olfactory receptor neurons, DA2 ORNs have bilateral projections to homologous glomeruli on both sides of the brain); the left hemisphere also contained 5 DA2 PNs (**fig 3A-B**). The same process was repeated for the single DL4 PN (**fig 3B**). We then marked up the presynaptic sites (a total of 1813 presynapses, 985 of which are in the right hemisphere) in the LH for all 10 DA2 PNs as a starting point for identifying their postsynaptic partners (see **fig S2A** for an example). Surprisingly, we found a significant number (n right side=25; n left side=27) of axo-axonic synapses from the DA2 PNs to the single DL4 PN in each hemisphere (**fig 3C-E, fig S2B**). As noted earlier, DL4 is activated by pheromone components of *Leptopilina* parasitoid wasps and also mediates oviposition avoidance [33]. The synapses appear to form clusters and are mostly located on the ventral branch of the PNs, as well as the point where the neurons split into the dorsal and ventral branches (**fig 3D**). Crucially, no other PN channel (of the remaining 49 uniglomerular excitatory PN types) receives more than 2 synaptic inputs from the DA2 PNs (**fig 3E**). In addition to this, the 5 DA2 PNs synapse strongly onto each other (n right side=42; n left side=37) (**fig 3E, fig S2B**), thus showing within-odour channel divergence and re-convergence that possibly serves to increase signal detection speed [42].

To assess whether the DA2 to DL4 synapses are a function solely of the close proximity of their axonal arbors or show further evidence of selective connectivity, we checked which other non-DA2 PNs pass within 1µm radius (>86% of PN axo-axonic synapses occur within this threshold) of DA2 output synapses in the LH. This revealed that, although other PN classes repeatedly pass close to DA2 synapses (DC2 being a notable example), DL4 is the only one to receive significant input (**fig S2C**). Thus, the ratio of observed to potential PN-PN connectivity is much higher for DA2-DL4 than other neighbouring PNs, further underlining the specificity of this connection. Behavioural valence-based axo-axonic integration of PN odour channels has not been described before, and might be an important mechanism for choosing similar behavioural responses to odours of similar significance to the fly.

We next searched for downstream LHN targets of the DA2 PNs using a sampling based strategy (see Methods for details). For this, we looked for neurons downstream of a single right-hand side DA2 PN. This approach identified a surprisingly large number of downstream targets: a total of 151 neurons (**fig 4A)** from 298 randomly sampled connections. The majority of these neurons were reconstructed to identification (i.e. sufficient to identify the overall morphology and class of the neuron, including soma and major branches) but not to completion i.e. omitting finer branches; this amounted to a total of 161 mm of traced cable. Nevertheless the combination of this random sampling along with extensive follow-up tracing (which identified 1729 connections to these 151 partner neurons out of an estimated total of 7310 DA2 output synapses, i.e. 24% complete) already allows us to draw some conclusions about the distribution of connection strengths and the diversity of cell types.

The identified partner neurons are morphologically diverse. We first classified them into 4 broad groups: olfactory PNs, local and output neurons of the LH (i.e. LHLNs and LHONs) and other neurons (**fig 4A**). More than half (61%) of the sampled synapses were onto LH output neurons (LHONs), and one fourth (24%) onto local neurons; this ratio of 2.5 is a good estimate of the relative connection strength of DA2 PNs onto the output (principal) neurons of the LH versus the local neurons. The olfactory PN group was the smallest (8 neurons, 7% of sampled synapses). Besides the DA2-DL4 interaction already described, the only other notable interaction was from DA2 PNs onto the axon terminals of a single inhibitory PN (2 random synapses, 13 total). Intriguingly the "other" group (n=12, 8%) included two presumptive taste PNs (with dendritic arbours in the suboesophageal zone) and a projection neuron innervating the VP4 dry air sensitive glomerulus [43]. All three received strong input on their axon arbours in the LH (27, 15, 23 total connections). Light level matches for these neurons can be viewed at virtualflybrain.org (VFB_00006745, VFB_00011799, VFB_00011086). This shows that the DA2 to DL4 axo-axonic connection described earlier is not unique, but that this pattern of connectivity can also be observed in select cross-modal interactions. A dry environment is likely a risk factor for eggs and newly hatched larvae; it is tempting to speculate that the taste PNs may respond to cues indicative of unfavourable egg laying sites.

To better understand the diversity of the remaining targets, we refined our coarse classification with hierarchical clustering of neuronal morphologies using NBLAST [32] (see methods). We used a single cut

bioRxiv preprint doi: https://doi.org/10.1101/394403; this version posted August 26, 2018. The copyright holder for this preprint (which was not certified by peer review) is the author/funder, who has granted bioRxiv a license to display the preprint in perpetuity. It is made available under aCC-BY-NC 4.0 International license.

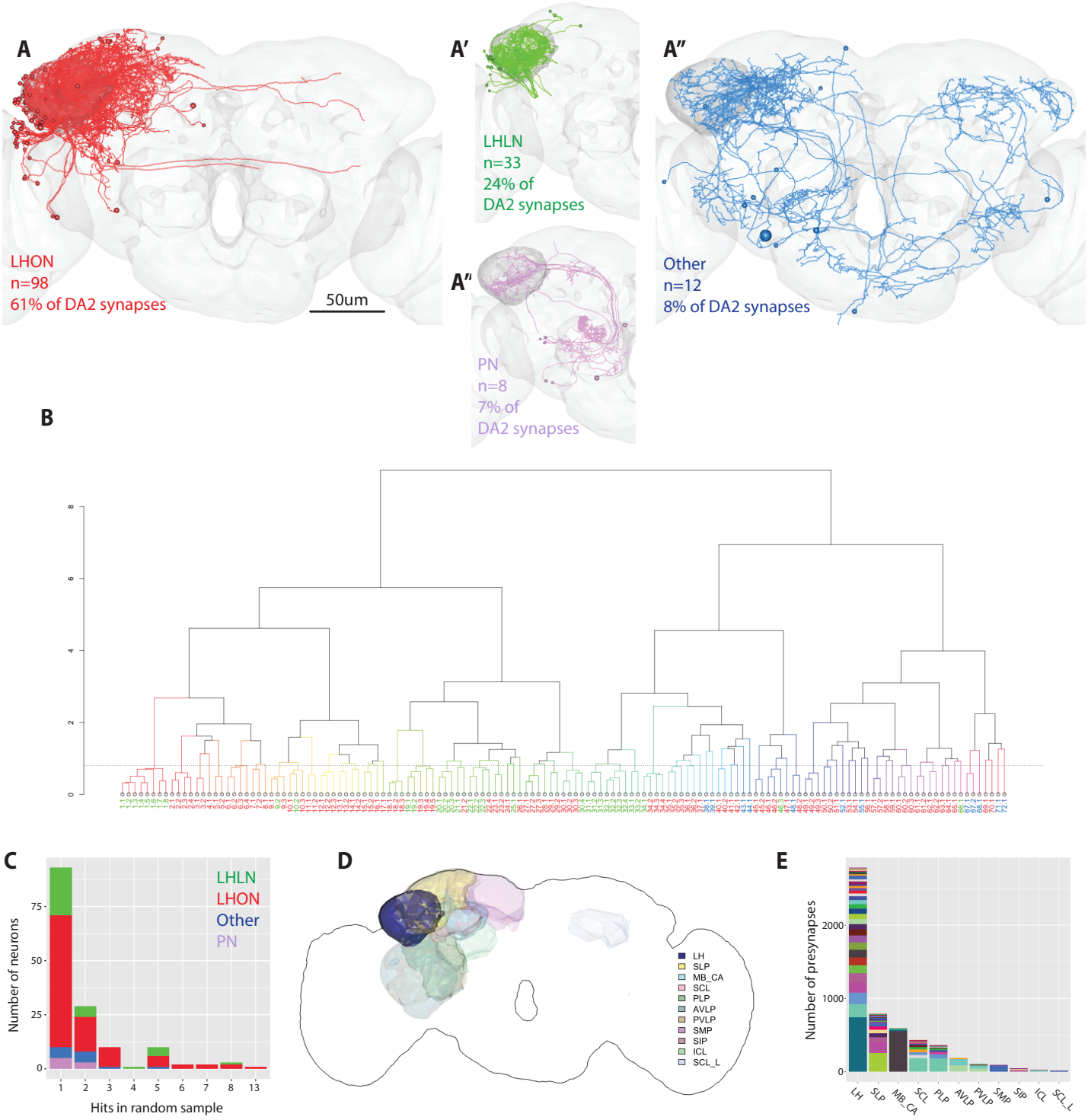

Figure 4: Extensive divergence of DA2 PNs onto multiple LHN targets.
(A-A‴) Downstream targets of DA2 PNs found by the random sampling in the LH shown in the FAFB template brain.
(B) Hierarchical clustering of the DA2 downstream targets (excluding PNs) based on NBLAST distance scores.
(C) Distribution of DA2 downstream target neurons by how many times they were hit in the random sampling, classified by broad neuron class.
(D) Neuropil regions targeted by LHONs downstream of DA2 PN. Colour intensity is based on the number of presynaptic connections in that neuropil.
(E) Number of presynaptic connections from LHONs downstream of DA2 PNs to different neuropil regions. Each LHON is uniquely colour-coded.
Neuropil regions for D and E are based on [45]. LH=lateral horn, SLP=superior lateral protocerebrum, AVLP=anterior ventrolateral protocerebrum, SCL= superior clamp, PLP=posteriorlateral protocerebrum, PVLP=posterior ventrolateral protocerebrum, SMP=superior medial protocerebrum, SIP=superior intermediate protocerebrum, MB_CA=mushroom body calyx, ICL=inferior clamp.

bioRxiv preprint doi: https://doi.org/10.1101/394403; this version posted August 26, 2018. The copyright holder for this preprint (which was not certified by peer review) is the author/funder, who has granted bioRxiv a license to display the preprint in perpetuity. It is made available under aCC-BY-NC 4.0 International license.

height of the resultant dendrogram tuned to identify anatomical (and likely functional) cell types based on our recent work ([44], see methods). This analysis divided 143 downstream partner neurons (identified from 287 randomly sampled connections) into 72 candidate cell types (**fig 4B**); note that this excludes 8 olfactory PNs connected via axo-axonic synapses. We provide a general summary of our results now and consider selected examples in greater detail in later results sections.

Local neurons (LHLNs) accounted for 9 of the identified groups while LHONs contributed to 53. The diversity of LHONs appears to be considerably larger than the number of local neurons, an effect that exceeds the 2.5 fold difference in output strength noted earlier. The top 4 LHLN groups accounted for 70% of the randomly sampled synapses. Exploratory analysis of these strongly connected groups identified three distinct patterns of connectivity. Group 1 (n=8 neurons) had arbours restricted to the domain of the DA2 axons, are mixed polarity neurons with extensive reciprocal connectivity. We inferred likely neurotransmitter phenotypes by comparing morphologies with a new split Gal4 collection for which neurotransmitter information is available (Dolan *et al.*, in preparation); this group contains PV4a12/PV4b2 cell types [44], which are glutamatergic. Group 32 (n=4) has arbours restricted to the medial domain of the DA2 axons, contains GABAergic neurons of the PV2 lineage and has weaker reciprocal connectivity. Group 22 contains a distinct class of PV4 neurons, also presumed glutamatergic, with polarised arbours that receive DA2 input and apparent axonal domains with widespread ramifications within the LH as well as the adjacent SLP region. These patterns suggest distinct computational roles – for example although group 1 and group 22 are both glutamatergic (a bifunctional transmitter though typically inhibitory in the fly CNS), the former may control the gain/dynamics of transmission from DA2 axons, while the latter may provide an additional computational layer within the LH between distinct pre and postsynaptic partner neurons.

We have already noted that we identified many more LHON than LHLN morphological clusters. Since the former also receive 2.5x more synapses, it could be that this disparity is because we identified a long tail of weakly connected LHONs. However we find that the strongly connected LHONs are also morphologically diverse. For example the 23 most strongly connected LHON groups (48 neurons) accounted for 70% of the synaptic budget (compare with 4 LHLN groups to reach the same proportion). We were somewhat less successful at positively inferring neurotransmitter phenotypes for the strongest LHONs, but many appear to be cholinergic and therefore excitatory although there were also examples of likely GABAergic or glutamatergic cells; this is in clear contrast to LHLNs where none of the strongest partners were cholinergic. The morphological diversity implied by our cluster analysis is matched by a corresponding diversity of LHON projections to various neuropil regions (**fig 4D-E**) thought to be involved in multimodal sensory integration [22,45–49] including the ipsilateral LH, superior lateral protocerebrum (SLP), anterior ventrolateral protocerebrum (AVLP), superior clamp (SCL), and the posterior-lateral protocerebrum (PLP). This distribution is similar to that recently described for LHONs at large [44,50] and includes convergence zones such as the SLP known to receive output from the mushroom body [17]. We examine specific examples in more detail below.

Our random sampling represents 21.3% of the total LH outputs for a single DA2 neuron (out of five per hemisphere). Obtaining a statistically rigorous estimate of the total number of DA2 partner neurons based on the random sampling data is challenging. Furthermore estimating the total number of partners without also obtaining information on their connection strengths would not be biologically meaningful – it is unlikely that partners receiving just one synaptic connection would have a significant behavioural impact. We therefore restrict ourselves to what we believe to be a conservative summary based only on existing tracing. We have identified (see AV1a1 Pigeon below) a behaviourally relevant neuron receiving a total of 7 DA2 inputs. If we use this as a threshold then 35 clusters (containing a total of 80 neurons) have at least one neuron known to receive this many connections. We anticipate that these numbers will increase markedly as future tracing increases the fraction of identified synaptic partners.

In summary, the geosmin processing pathway, which shows a labelled line organisation in the sensory periphery, shows convergence with the behaviourally related DL4 PN channel at the level of PN axons, as well as considerable divergence at the transition from second to third-order neurons. The wiring logic of the LH therefore appears to be considerably more complex than suggested by light microscopy studies of pheromone pathways [22,23]. PNs carrying odour information of similar behavioural meaning do not synapse onto just a small number of shared postsynaptic targets.

Convergence of aversive PN channels

As all the PNs on the right hemisphere had been completed at this point, tracing out the LHNs allowed us to identify inputs from all 51 olfactory glomeruli, including the remaining 4 DA2 PNs that were not used for the sampling. We could also compare the number of synaptic connections found by random sampling to the total number of synaptic connections: even though most of the neurons were seen to receive only a single connection to the DA2 PN in our random sampling (**fig 4C**), the majority of these were now shown to actually be multiply connected (**fig S2E**). For the subset of LHNs that we traced to completion, the median number of DA2 inputs from all 5 PNs was ~10 even for the neurons that received only a single connection in the random sampling. Additionally, the neurons that received multiple hits in the random sampling were found to be, on average, more highly connected overall.

The large number of DA2 targets precluded a comprehensive analysis of all pathways. We therefore selected a few LHNs for further study based on the extent of DA2 input, availability of genetic reagents (see below) or distinctive anatomical features. We first examined AD1a3 Aspis, one of the strongest DA2 downstream targets (most strongly connected after initial ~10% random sampling, tied second place after ~20%) (**fig 5A)**. AD1a3 is a systematic identifier that defines a cell type within a comprehensive LHN nomenclature that we have recently established [44]. Aspis is a unique identifier given to the single cell of this class identified on the fly's right within the full adult female EM volume.

Aspis receives in total 108 synaptic inputs from all 5 DA2 PNs of the right hemisphere and projects to the superior intermediate protocerebrum and superior lateral protocerebrum. Interestingly, this still only represents ~1.6 % of the total synapses that DA2 PNs make in the LH. While it receives strong input from DA2, DC2 (that has been reported to respond to multiple aversive odorants, including benzaldehyde [35], but also to other odours [51]), and DC4 (aversive protons [52]), it also receives strong input from a relatively broad set of PN channels of varying valence (**fig 5B,C**), making it an unlikely candidate for specifically integrating aversive input.

LHN cell type PV6a3 [44], represented by the neuron Caligari in our dataset, is another strong DA2 downstream target: it is tied with Aspis for connections found in the random sampling, and the third strongest DA2 target overall with a total of 68 synaptic inputs (~1.0 % of the DA2 synapses in the LH). The dendrites of this neuron cover the same crescent shaped area of the LH associated with aversive PN axons (compare **fig 5A'** with **fig 2C-D**), and its axons project to the superior lateral protocerebrum. It receives a sparse set of PN inputs (**fig 5B'&C**): only 5 PN classes provide >10 synapses. Interestingly, among these 5

bioRxiv preprint doi: https://doi.org/10.1101/394403; this version posted August 26, 2018. The copyright holder for this preprint (which was not certified by peer review) is the author/funder, who has granted bioRxiv a license to display the preprint in perpetuity. It is made available under aCC-BY-NC 4.0 International license.

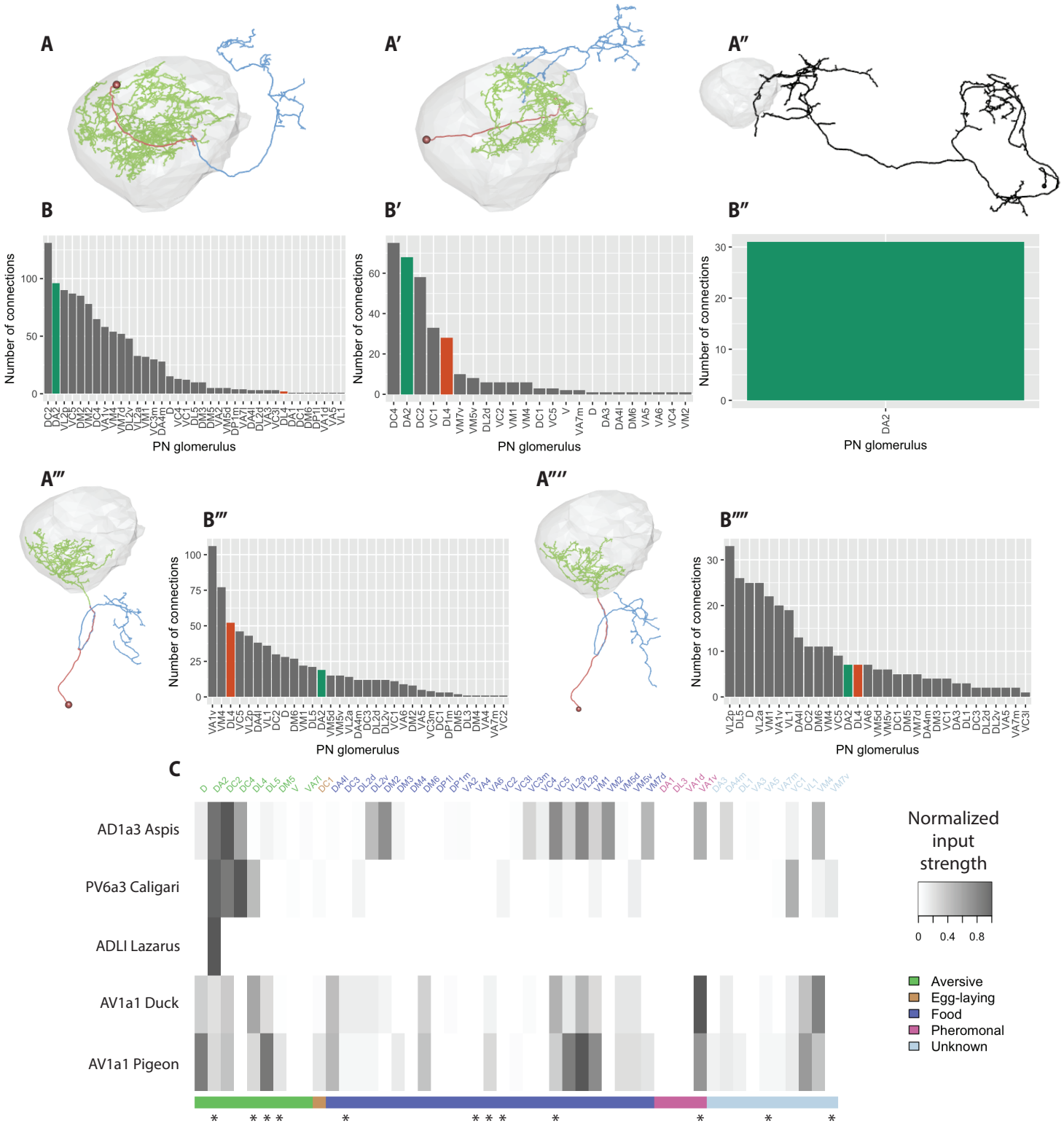

Figure 5: Some DA2 downstream targets receive input from multiple aversive PN channels.
(A-A⁗) Morphologies of five DA2 downstream targets of special interest. (A) Aspis (n synapses from DA2 PNs=108). (A′) Caligari (n=68). (A″) Lazarus (n=31). (A‴) Duck (n=19). (A⁗) Pigeon (n=7). Cell bodies and primary neurites are coloured red, dendrites green, and axons blue, where such a division was possible.
(B-B⁗) Number of synaptic inputs onto Aspis (B) Caligari (B′), Lazarus (B″), Duck (B‴), and Pigeon (B⁗) by PN type.
(C) Heatmap representation of PN to selected LHN connectivity, normalised by the total PN inputs to each neuron, and colour-coded by putative behavioural relevance [12,33,35,36,51,52,54]. Odour channels implicated in aversive behaviour, specifically in an egg-laying context, are marked with asterisks [12,33,38,58].

bioRxiv preprint doi: https://doi.org/10.1101/394403; this version posted August 26, 2018. The copyright holder for this preprint (which was not certified by peer review) is the author/funder, who has granted bioRxiv a license to display the preprint in perpetuity. It is made available under aCC-BY-NC 4.0 International license.

there are several PN classes that are thought to carry aversive odour information: DC4 [52], DC2 [35,51], and DL4 (parasitic wasp pheromones [33]). Thus, this LHON appears to be an ideal candidate to perform valence-based integration, a computation we hypothesised might take place in the LH. Unfortunately, the neuron does not morphologically match any previously described neurons, and we were unable to find a driver line targeting it.

Thirdly, a large, brain spanning neuron Lazarus receives strong bilateral synaptic input from DA2 PNs in the LH (right side=31, left side= 19, ~0.5% of DA2 synapses in the LH), and sends bilateral projections to the calyx of the MB, as well as PLP, SLP, AVLP, SCL, inferior clamp, and superior medial protocerebrum (**fig 5A''**). Strikingly, DA2 PNs are its sole source of uniglomerular PN input in the LH (**fig 5B''&C**). An NBLAST [32] search against the FlyCircuit database [31] found a good match for the neuron (**fig S2F**). Based on the morphology and the presence of neuropeptidergic dense core vesicles (**fig S2G**), Lazarus is likely to be the ADLI neuron described in [53], which expresses natalisin, a neuropeptide widely conserved in arthropods, potentially involved in reproductive behaviours.

Finally, we identified two type AV1a1 [44] LHONs: Duck and Pigeon (**fig 5A'''&A''''**). These LHONs receive strong (Duck) to moderate (Pigeon) input from both DA2 and DL4 PNs (**fig 5B'''&B''''**). For Duck, we found 19 synaptic connections from DA2, and 51 from the single DL4 PN (**fig 5B'''**), making it the second strongest downstream target of DL4 PNs. Pigeon received 7 synaptic connections from both DA2 and DL4 PNs (**fig 5B''''**). Combined, these neurons receive ~0.4% of the DA2 synapses in the LH. Although, as mentioned above, DA2 PNs also synapse onto DL4 PNs, putatively providing a somewhat higher level of input to these neurons than what is suggested by the number of synapses from DA2 PNs alone. However, AV1a1 neurons receive a relatively broad set of PN inputs (**fig 5B'''-B'''' & fig 5C**) including the supposedly aversive (DL5, DC2, D [35,51]), food [51,54] and even pheromonal inputs (VA1v [55]) (although notably, activating the VA1v pathway in isolation was recently shown to be strongly aversive in an egg-laying context [38]). Interestingly, many of the strongly connected food related PNs (VC5,VL2a, VL2p, VM1) receive sensory information via the family of ionotropic IR receptors [56]. These mainly respond to acids and polyamines [57]. The latter have been shown to be attractive in a T-maze but aversive in an egg-laying context (although this may involve the gustatory system) [58].

While the AV1a1 neurons were not the strongest targets of DA2 PNs, nor as selective to it as some of the other LHNs, there are nevertheless a few factors that make them particularly interesting. Firstly, the same neuron type (AV1a1) came up in our sampling twice (Duck and Pigeon). Secondly, morphologically similar neurons have been suggested to be important for aversive odour processing based on functional imaging experiments performed on a relatively broad driver line [59]. Thirdly, the dendrites of the neurons arborise in the ventral-posterior LH where most aversive PNs send their axonal projections. A recent paper, using a novel olfactogenetic approach suggests that this area of the LH may mediate negative egg-laying decisions similar to the avoidance of geosmin [38]. A statistical cross-comparison of the AV1a1 inputs and the odour channels recently reported to be most aversive in an egg-laying context [38] shows that both neurons receive more inputs from aversive channels than would be expected by chance: Duck receives strong (>10 synapses) input from 3/5 of the most aversive PNs (VA1v, DL4, DL5 but not VC2, VA3), and only 3/19 from the rest (Chi-squared test p=0.04); For Pigeon the numbers are 2/5 (VA1v, DL5,) and 1/19, respectively (Chi-squared test p=0.04).

Thus, in summary, despite the considerable divergence of DA2 onto many LHN targets, we find neurons that receive inputs from multiple aversive PN channels, and could in principle act as valence based integrators for behavioural aversion either in an egg-laying context or more generally (see **fig 5C** for overview).

Light-level in silico *anatomical screen for DA2 downstream targets finds cell type-specific driver lines*

For our parallel light-level screening for DA2 downstream neurons and driver lines, we used registered confocal stacks of R85E04 converted into a binary mask showing the axonal projections pattern of the PNs in the LH (**fig 6A**). This mask was then co-visualised together with Janelia FlyLight GAL4 lines [28] that had been annotated to have expression in the LH (a total of 351 GMR lines annotated by Frechter *et al.* [44]) (see **fig 6B-C** for an example). The GMR lines were then manually scored for amount of overlap (reflecting the *a priori* probability of synaptic connectivity), and sparseness of expression pattern (allowing better identification of LHN cell type and more specific targeting of LHN types). For most of the best candidate LHN types we were also able to identify a Split-GAL4 line from a collection being made as a part of an ongoing effort to create a comprehensive cell type-specific driver line library for LHNs (Dolan *et al.*, in preparation). Overall, the *in silico* screen narrowed down the number of putative DA2 downstream targets to 18 LHN types, 12 of which could be accessed relatively specifically through either GAL4 or Split-GAL4 lines (details will be described in Dolan *et al.*, in preparation).

AV1a1 LHNs found in LH728 and LH1983 trigger aversion and are necessary for geosmin avoidance in egg-laying

To look for behaviourally relevant LHNs potentially downstream of DA2 PNs, we next carried out a behavioural optogenetic activation screen on the hits of the *in silico* anatomical screen for aversion triggering LHNs. As the Split-GAL4 lines in most cases had stronger expression levels as well as less off-target expression, they were used instead of the GMR GAL4 lines where possible. A total of 27 driver lines (for 12 LHN types) were tested (the full details of the screen in Dolan *et al.*, in preparation). The behavioural experiments were carried out similarly to [17], using a four-field arena (**fig 6D**), and only female flies were used for the screen. However, only two of the tested driver lines that had LHNs putatively downstream of DA2 PNs triggered aversion in this assay (in comparison to the mildly phototactic genetic control Empty-Split GAL4) (**fig 6E, S3A-C**): LH728 and LH1983 (**fig 6F-G**). Both Split-GAL4 lines shared a parent line (R22D02, **fig 6B**) and appear to label a small group of neurons with their somas ventral and medial to the ventrolateral protocerebrum (AVLP). Both lines appear to contain the same two strongly labelled neurons sending dendrites to the (ventral) LH and axons to the AVLP, and no other LHNs. These LHNs belong to the neuron type AV1a1 according to a recent LHN annotations [44], are cholinergic (Dolan *et al.*, in preparation), and appear morphologically very similar to the AV1a1 neurons Duck and Pigeon found downstream of DA2 PNs in the EM sample (**fig 6H**).

To quantitatively match the neurons labelled by LH728 and LH1983 to the EM tracings we generated light-level tracings of the neurons in LH1983. LH1983 was used for this as the signal to noise ratio of the line was deemed better (see **fig 6F-G**). As the processes of the two LHNs were in many places too close to resolve, the tracing resulted in a single hybrid skeleton of the two AV1a1 neurons found in the line. However, overlaying the light-level tracing (black) with Duck and Pigeon (green, magenta) reveals remarkably similar morphology (**fig 6I**). Moreover, a quantitative comparison of morphology between the light-level tracing and all the 33 neurons taking the AV1 tract using the NBLAST algorithm [32] shows that the top matches are Duck (NBLAST similarity score=0.69) and Pigeon (NBLAST similarity

bioRxiv preprint doi: https://doi.org/10.1101/394403; this version posted August 26, 2018. The copyright holder for this preprint (which was not certified by peer review) is the author/funder, who has granted bioRxiv a license to display the preprint in perpetuity. It is made available under aCC-BY-NC 4.0 International license.

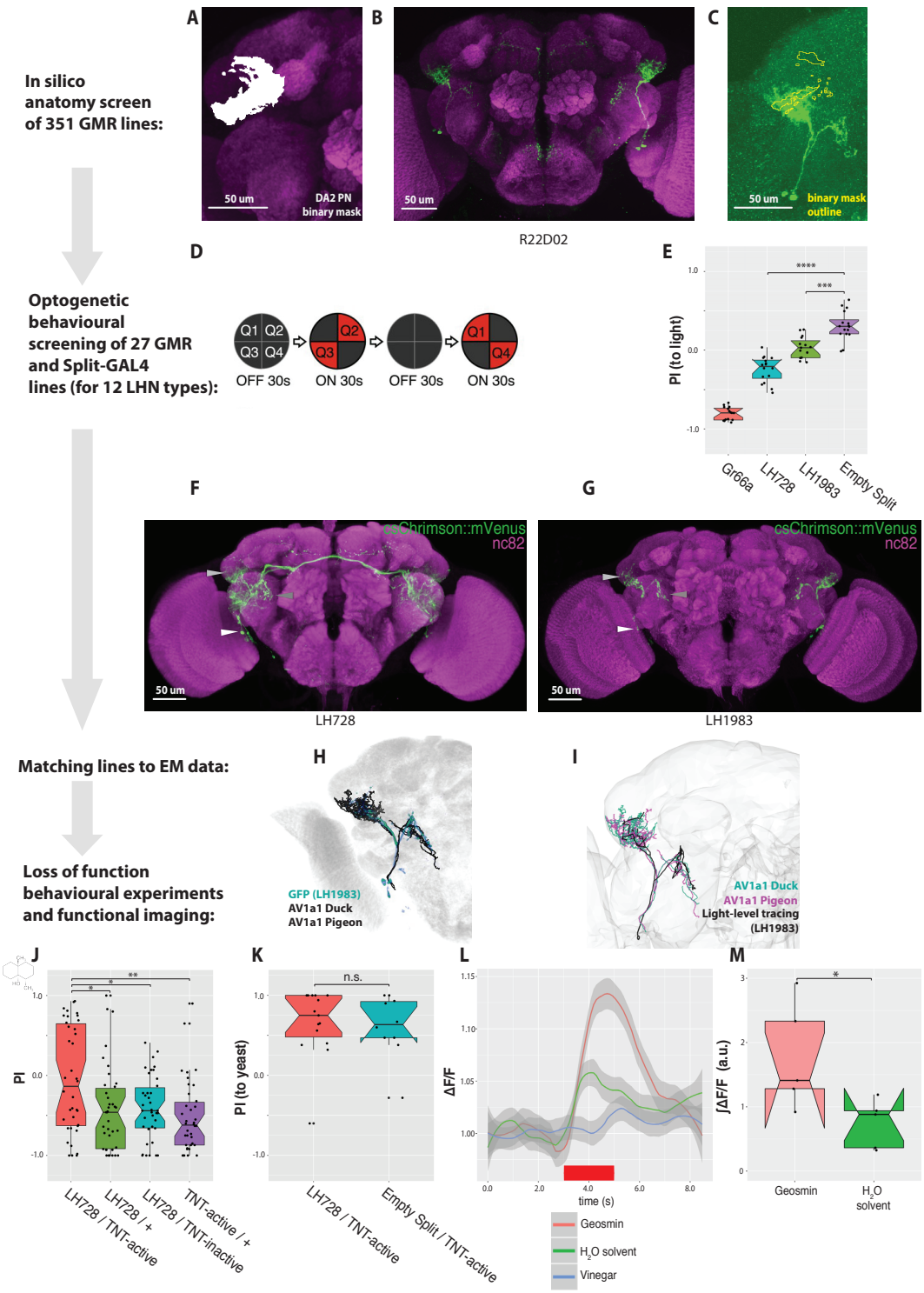

Figure 6: Identifying Split-GAL4 lines labeling DA2 PN downstream targets.
(A) An LH close-up of the binary mask generated from registered confocal images of DA2 PNs (R85E04) axonal projections (JFRC2 template brain).
(B) An example of a good hit (R22D02) in the in silico screen. A maximum intensity projection of a confocal stack (JFRC2 template brain).
(C) An example of the binary mask (as an ROI, in yellow) together with a GAL4 driver line (R22D02, expression pattern in green). A partial projection (JFRC2 template brain).
(D) A schematic representation of the optogenetic four quadrant assay [17] used for behavioural screening. 20 female flies explore a circular arena for 30 seconds before two of the quadrants are illuminated with red light for 30 seconds, after which the protocol is repeated by illuminating the remaining two quadrants.
(E) PI (to the light quadrants) for the last 5 seconds of the stimulation epochs. Two split-GAL4 lines (LH728 and LH1983) are compared to the parental control via two-sample t-tests with Holm-Bonferroni corrections for multiple comparisons. Gr66a-GAL4 shown as a positive aversive control.
(F-G) Expression patterns of LH728 and LH1983 (JFRC2013 registered maximum intensity projections of female brains). The arrowheads mark the cell bodies (white), dendrites (light grey), and axons (dark grey) of the type AV1a1 LHNs.
(H) A 3D rendering of EM reconstructions of Duck and Pigeon (black) overlaid with the LH1983 expression pattern (green). Bridging registrations were used to transform the EM skeletons into the JFRC2013 reference brain.
(I) A light-level tracing of the AV1a1 LHONs from LH1983 (black) overlaid with EM-level tracings of Duck and Pigeon (green and magenta, respectively) in the JFRC2013 reference brain.
(J) Egg-laying two-choice preference indices (PI) to geosmin while silencing putative DA2 downstream targets by expressing tetanus toxin light-chain (TNT) [30] via LH728 (groups compared by a Kruskal-Wallis rank sum test followed by post-hoc comparisons of experimental group to each of the parental groups by Wilcoxon rank sum tests with Holm-Bonferroni corrections. n=38 for all groups).
(K) Egg-laying two-choice preference indices (PI) to yeast odour (groups compared by a Wilcoxon rank sum test with continuity correction).
(L) Odour-evoked in vivo two-photon imaged calcium responses (GCaMP3.0) from LH dendrites of AV1a1 neurons labelled by LH728 (n=5).
(M) Area under curve for the stimulation epoch for geosmin and its solvent control (green). Data same as L. (Paired samples t-test, n=5).
Significance values: * $p<0.05$ ** $p<0.01$ *** $p<0.001$ **** $p<0.0001$

bioRxiv preprint doi: https://doi.org/10.1101/394403; this version posted August 26, 2018. The copyright holder for this preprint (which was not certified by peer review) is the author/funder, who has granted bioRxiv a license to display the preprint in perpetuity. It is made available under aCC-BY-NC 4.0 International license.

score=0.65), respectively (**fig S3D**). Taken together with the fact that no other AV1 tract neuron appears to get significant amount of synaptic input from DA2 PNs, these data strongly suggest that the LHNs in the driver lines are in fact the AV1a1's Duck and Pigeon.

As type AV1a1 neurons were the only putative downstream targets of DA2 PNs that triggered aversion in our optogenetic screen, we wanted to characterise their role in geosmin avoidance behaviour in more detail. Silencing the synaptic activity of the neurons by expressing the tetanus toxin light chain via LH728 resulted in a loss of geosmin avoidance in the egg-laying two-choice assay (**fig 6J**). Thus the AV1a1 neurons appear to be not only sufficient to cause aversion when activated, but also necessary for the geosmin aversion response, suggesting that they are a key node in the circuit. As the loss of function phenotype could in principle be explained by the silencing of AV1a1 neurons causing a general deficit in olfactory sensing or odour guided behaviours, we tested whether the same flies could still respond to other odours in a similar task. However, silencing the AV1a1 neurons via LH728 had no effect on attraction to yeast odour in the egg-laying two-choice assay (**fig 6K**). Finally, we also tested whether the AV1a1 neurons found in LH728 respond to odour stimulation with geosmin. As we deemed the cell-bodies of the neurons to be too ventrally located to be accessible by *in vivo* electrophysiology, we opted to use *in vivo* two-photon microscopy to image the activity of the GCaMP3.0 calcium reporter [60] in the LH dendrites instead. The functional imaging revealed relatively small but significant responses to geosmin, but not to vinegar (a broadly coded attractive odorant) (**fig 6L-M**).

In summary, the light-level screening allows us to identify and target a small group of LHNs (type AV1a1), show that they are sufficient to trigger aversion, confirm that they respond to geosmin, and are necessary for geosmin aversion in the context of egg-laying. We were also able to match the neurons in the driver lines to the neurons traced in the EM volume, and thus unify the two parallel approaches taken to find DA2 downstream targets in the LH.

Further downstream tracing from the LH identifies descending neurons

The considerable divergence of the geosmin processing pathway at the 2nd to 3rd order level means that within the scope of this work we are unable to follow all of the connected LHNs deeper into the brain. Instead we chose to focus our efforts on a small number of LHONs we judged to be of special interest. As Aspis (AD1a3) was thought to be too broadly tuned (receiving input from almost half of the uniglomerular PNs) (**fig 5B**), and we observed dense core vesicles in Lazarus (**fig S2F**), raising the possibility of it acting on its downstream

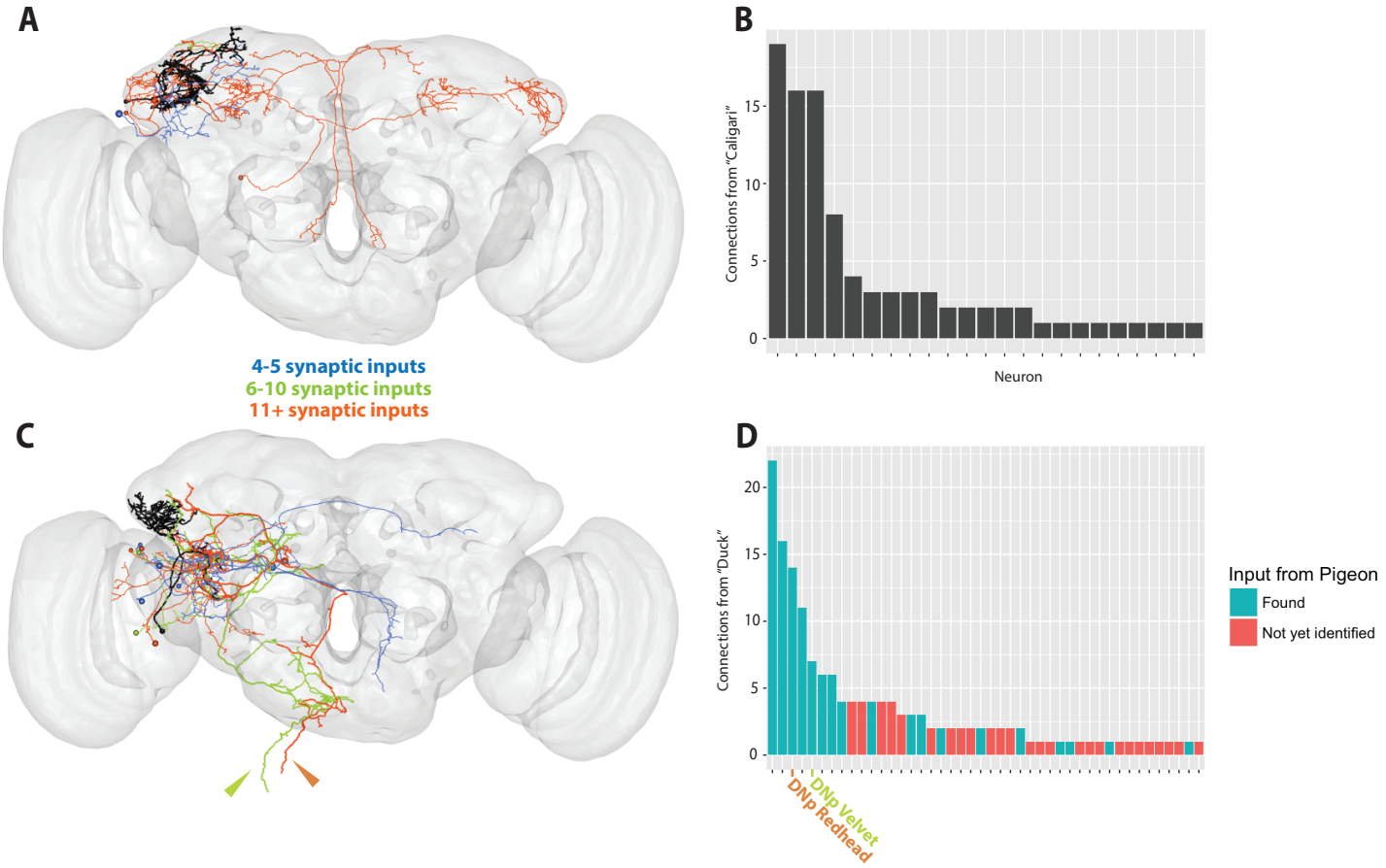

Figure 7: Downstream targets of geosmin sensing LHONs.
(A) Identified downstream targets of PV6a3 Caligari with 4 or more synaptic inputs. Neurons are colour-coded based on connection strength: 4-5 synapses=blue; 6-10=green; 11+=orange.
(B) The number of synaptic inputs from PV6a3 Caligari to all identified downstream targets.
(C) Identified downstream targets of the AV1a1 Duck with 4 or more synaptic inputs. Neurons are colour-coded similarly to A. Two descending neurons DNp Redhead (orange) and DNp Velvet (green) are highlighted with the arrowheads.
(D) The number of synaptic inputs from "Duck" to its downstream targets. The two descending neurons are highlighted. The neurons that receive input from the other AV1a1 neuron Pigeon are marked in cyan.

bioRxiv preprint doi: https://doi.org/10.1101/394403; this version posted August 26, 2018. The copyright holder for this preprint (which was not certified by peer review) is the author/funder, who has granted bioRxiv a license to display the preprint in perpetuity. It is made available under aCC-BY-NC 4.0 International license.

targets through volume transmission-based neuromodulation, we opted to focus on Caligari (PV6a3) and Duck, the stronger of the two AV1a1 neurons receiving DA2 input.

Caligari (PV6a3) receives strong input from DA2 (n of synapses=68), as well as from a number of other aversive PN channels (DC4, DC2, and DL4) (**fig 5B'**). Interestingly, it also appears to be selective to them, making it an ideal example of an LHN that integrates odour channels of similar valence. In order to explore how the integrated aversion signal is transformed into behaviour in the fly brain we traced further downstream from Caligari by the random sampling approach (**fig S4A**). We identified 14 postsynaptic partners receiving 2 or more synapses, the strongest of which appears to be a neuron projecting to the subesophageal zone (**fig 7A-B**). It is therefore possible that at least part of the next computational step in the circuit is to integrate the aversive odour signal with gustatory signals.

While Duck and Pigeon do not receive input solely from PN channels thought to be aversive, they appear to be especially important for transforming the sensory input into a behavioural response. Downstream sampling from the Duck axons in the VLP reveals a variety (n=44) of postsynaptic partners (**fig 7C-D**), many of which were also observed to receive input from the other AV1a1 neuron Pigeon. Perhaps most notably, we find two descending neurons DNp Redhead and DNp Velvet projecting to the ventral nerve cord (**fig 7C**, highlighted by the orange and green arrowheads). Both of these descending neurons also receive input from Pigeon. This suggests that the shortest path from antennal ORNs to the neurons directly involved in motor control might be as few as 4 synapses in this circuit.

Discussion

Innate odour-guided behaviours in *Drosophila* have long been thought to depend on the LH [19]. However positive evidence for this has been lacking, in large part due to the absence of genetic reagents to target third order LHNs. Here we characterise the innately aversive geosmin processing pathway from peripheral sensory neurons through PNs and LHNs all the way to 4th order DNs by a combination of light- and EM-level neuroanatomy, behavioural experiments, electrophysiology, and functional imaging. We identify behaviourally relevant PNs and LHNs (i.e. 2nd and 3rd order neurons), and observe a significant divergence of the pathway at the level of PN to LHN connectivity, as well as convergence of multiple aversive pathways onto the same LHN targets. Some of these LHN targets go on to synapse onto descending 4th order neurons that project to the nerve cord, suggesting that the shortest path from sensory to motor neurons could be as short as 4 synapses (see **fig 8** for summary).

Axo-axonic convergence of aversive signals

We describe, for the first time to our knowledge, the presence of axo-axonic synapses between olfactory PNs. The connection seems to be specific between DA2 and the parasitic wasp-pheromone-processing DL4 PNs: there are numerous other PNs in the vicinity of DA2 synapses with which they could potentially connect, but do not. This convergence only happens at the LH, after the axons have passed the MB. Thus the two channels can in theory be separate for the purposes of learning, but still converge for hard-wired responses. The functional significance of these synapses is not yet clear, but it seems likely that the excitatory input from DA2 PNs will make DL4, and its downstream targets, more likely to fire if the DA2 channel is active as well. The synapses are localised primarily in the ventral branches of the PNs, as well as the point where axons split into the ventral and dorsal branches (**fig 3D**). Furthermore, they are organised into clusters, which should facilitate the summation of synaptic potentials by the DL4 neurons. Notably, the connections are almost exclusively unidirectional: DA2 onto DL4 suggesting that part of the DA2 response could be organised through DL4 downstream circuiry.

This organisation could be a consequence of developmental timing (DL4 is an embryonic born PN [61], whereas DA2 develops later [62]). Also, larvae avoid wasp odours [33], but not geosmin, and indeed lack the receptor for it), or evolutionary order of arrival, so that later arriving PN channels engage existing circuitry. Finally, as synapses are energetically very costly even compared to the rest of the brain [63,64], convergence already at the level of PNs seems like a cost-efficient solution to the problem of energy-information tradeoffs [65,66]. Our unpublished observations (Schlegel, Bates *et al.*, in preparation) have found that there are numerous other axo-axonic PN interactions, that these are largely unidirectional, and specifically link behaviourally related groups of PN channels. Thus, convergence of similar odour channels seems to take place in the LH, but this already happens at the level of second order olfactory neurons.

Extensive divergence of the geosmin pathway in the LH

The arrival of DA2 PNs in the LH appears to demarcate the end of 'labelled line' encoding: DA2 PNs synapse onto a large and diverse population of LHN targets, many of which receive input from multiple classes of PNs. Previous work based on functional experiments and light microscopy [22,23], together with the similar PN axon morphologies of related odour channels [20,33,67], has suggested that the path from smell to behaviour might be quite direct for innate responses. The observed massive broadening of the circuit shows that this view of the LH is too simple: while the downstream networks may not be particularly deep in terms of synaptic layers, they are clearly broad. However, the number of DA2 target LHNs is perhaps only surprising when thinking of behavioural responses to odours in an equally oversimplified, unidimensional (attraction-aversion, measured by preference indices) manner. Odour valence has been a useful concept for studying how sensory responses are transformed into behaviour, and how memory works, but we need to develop a more multidimensional view of what a behavioural response to an odorant is, and what it requires of the animal computationally. Odour identity and valence (in its simplest sense) are not enough for the fly to produce an appropriate behavioural response: rather this is a process of dynamic sensory-motor integration using variables such as wind direction [24,68,69], changes in concentration as a function of time, internal context [25,70], and previous experiences [71,72]. Furthermore, the behavioural response, manifesting itself in attraction or aversion, is in fact a more complex combination of turns and straight runs [73,74] orchestrated by the neural circuits downstream of PNs and LHNs. Further work with cell-type specific manipulations of connected LHNs, together with higher spatiotemporal resolution behavioural assays, could aid in determining the exact roles of the connected neuron types, and how they enable the fly to avoid an odour source. Finally, as the animal is unable to do two things simultaneously, some local LHNs might serve to cross-inhibit other odour channels, perhaps resulting in a winner-take-all type of responses in LH and downstream neurons. Determining the neurotransmitter profiles of the neurons will therefore also be an important step forward.

Convergence of aversive signals on LHNs

Despite the considerable broadening of the 'labelled line' within the LH, we identify LHNs that based on behavioural or connectivity data may be key nodes in the circuit. One example is the PV6a3 LHN Caligari, which, based on its PN inputs, appears to confirm our starting hypothesis for LHNs downstream of DA2 PNs: it integrates several

bioRxiv preprint doi: https://doi.org/10.1101/394403; this version posted August 26, 2018. The copyright holder for this preprint (which was not certified by peer review) is the author/funder, who has granted bioRxiv a license to display the preprint in perpetuity. It is made available under aCC-BY-NC 4.0 International license.

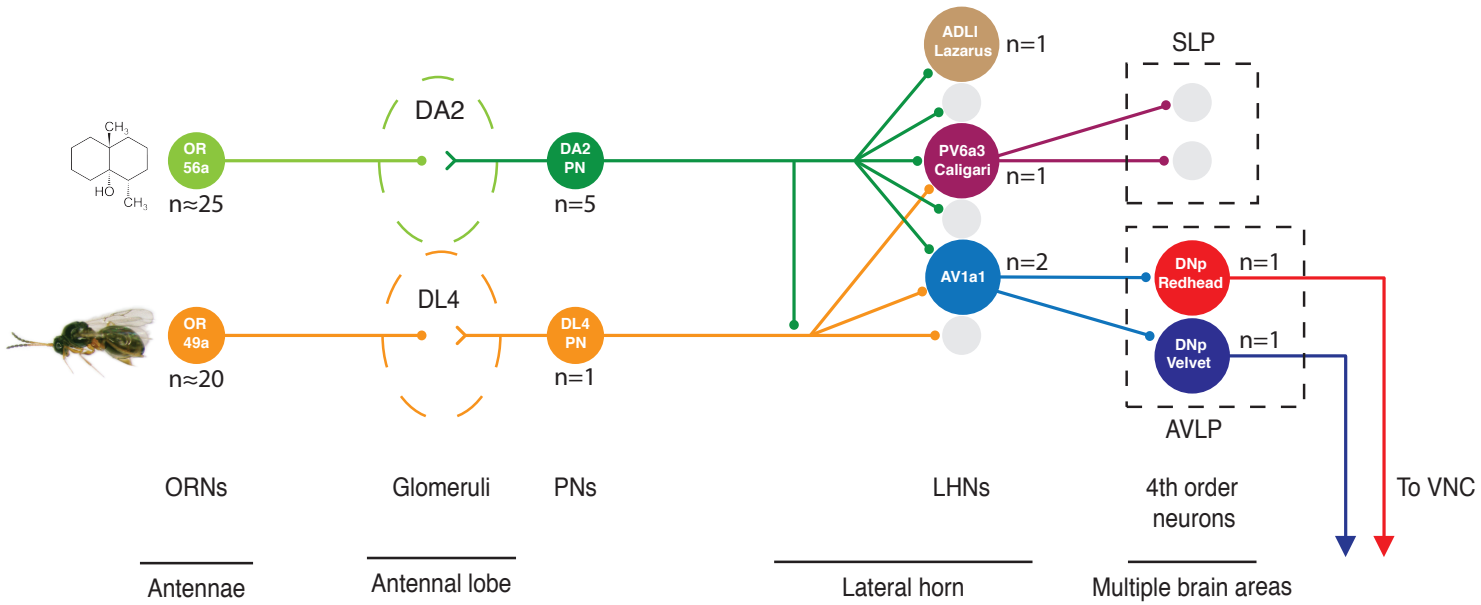

Figure 8: A schematic circuit model of geosmin processing
Geosmin is detected by ORNs expressing the OR56a receptor, housed in the ab4 sensillae of the antennae (left). The ORNs project to the AL where they converge onto 5 PNs, as well as local neurons (not shown), in the DA2 glomerulus. The DA2 PNs then go on to project to the LH, forming *en passant* synapses onto the Kenyon Cells of the MB on the way (not shown). In the LH the DA2 PNs form axo-axonic synapses onto each other (not shown), and the single aversive, parasitic wasp pheromone responsive DL4 PN. They also synapse onto a total of 80 3rd order neurons, some of which receive PN input only from DA2 (the neuropeptidergic ADLI Lazarus), some which appear to integrate input only from aversive PNs (PV6a3 Caligari), and some that receive input from multiple aversive PNs, but also non-aversive PNs (AV1a1 Duck and Pigeon). The latter are, although only receiving ~0.4% of the total synaptic inputs that DA2 PNs make in the LH, sufficient to trigger aversion when artificially activated, as well as necessary for geosmin aversion in the egg-laying context. The pathway then diverges further, onto multiple 4th order target neurons, some of which are DNs sending their axons to the nerve cord. Numbers of neurons are marked where there is more than one neuron of the same type.

aversive inputs. However, until a driver line labeling the neuron is identified, we are unable to probe its functional role. Another interesting example is ADLI Lazarus, one of two neurons in the brain releasing the natalisin neuropeptide [53]; it receives olfactory input in the LH exclusively from the DA2. Previous work on manipulating natalisin levels pan-neuronally, or natalisin expressing neurons via *ntl*-GAL4 result in male courtship and female receptivity reductions [53]. Although manipulating the ntl-expressing neuron activity did not show any egg-laying behavioural phenotypes in *Drosophila,* a knock down of ntl in the red flour beetle *T. castaneum* resulted in a reduced number of eggs laid, although the origin of this phenotype was not clear [53]. In any case, the extremely specific set of inputs in the LH makes this neuron somewhat of an anomaly, and therefore intriguing.
Finally, we identify the AV1a1 LHNs (Duck and Pigeon) which, although not exclusive to aversive PN input, do appear to integrate information from multiple aversive odour channels, respond to geosmin, and are necessary for geosmin avoidance in an egg-laying context, as well as sufficient to cause avoidance when artificially activated. Despite the activation phenotype, whether AV1a1 neurons in fact are under normal circumstances only relevant for olfactory avoidance in an egg-laying context, or controlling aversion more generally is unclear for the time being. However, the fact that the synapses from DA2 PNs to AV1a1 neurons represent only ~0.4% of the DA2 synapses in the LH, but silencing the neurons results in complete abolishment of the egg-laying aversion, lead us to think they might be selectively required in this context. This view is also supported by the observation that the neurons get strong input from PN channels that have been shown to be specifically aversive in the egg-laying context (such as DL4), or have even been shown to be attractive in other assays (VA1v) [55], but appear to be aversive in the egg-laying context [38]. Indeed, as mentioned above, these neurons receive more egg-laying aversion related inputs than would be expected by chance. If the role of the AV1a1 is in fact limited to the egg-laying context, the other DA2 input receiving LHNs might then be required for some other olfactory-guided behaviours, such as long-range aversion. Thus the multitude of LHN types downstream of the PN channel could exist to match the number of behavioural options that the animal has. Other external and internal information would then perhaps result in only one or few of these postsynaptic neurons being activated at a time.
Further behavioural experiments together with cell-type specific manipulations should be able to clarify this.

Odour inputs onto descending neurons

By tracing downstream of the AV1a1 LHNs we identify interneurons descending to the ventral nerve cord. This suggests that while the transition from smell to behaviour for aversive odours may involve a much broader repertoire of higher olfactory neurons than previously thought, at its shallowest it may have the same number of synaptic levels (minimum of 4) as suggested previously for pheromone responses [22]. This is one synapse fewer than what is thought to be the case for escape responses triggered by visual stimuli in *Drosophila* [75], possibly reflecting the increased relative complexity of the visual computations needed to react to a rapidly *approaching* object. It is also worth noting that the olfactory information receiving DNs have some of their arbours very close to the giant fiber DNs involved in visual escape behaviours. An intriguing possibility would be that under certain conditions, for example when landing on a noxious microenvironment,

bioRxiv preprint doi: https://doi.org/10.1101/394403; this version posted August 26, 2018. The copyright holder for this preprint (which was not certified by peer review) is the author/funder, who has granted bioRxiv a license to display the preprint in perpetuity. It is made available under aCC-BY-NC 4.0 International license.

strong aversive olfactory signals could actually trigger the animal to take flight, as is the case with a looming visual stimulus. The DNs identified here could in principle either trigger a stereotyped behavioural response (as appears to be the case with the escape behaviour triggering DNs) in a command neuron-like manner, or they may be part of a population of, potentially multipurpose, DNs that guide behaviour in a more flexible manner.

General properties of the circuit

Looking at the circuit as whole (summarised in **fig 8**), we observe a few general properties, that may reflect what happens in other sensory pathways in the fly brain, or elsewhere: First, at each level of the circuit the number of non-unique parallel elements (similar neurons, such as Or56a ORNs or DA2 PNs) appears to decrease, while the number of unique parallel elements increases (number of cell types in each layer). In more concrete terms, ~25 similar Or56a ORNs [14] synapse onto 5 DA2 PNs and local neurons, and the 5 PNs then synapse onto ~150 3rd order neurons of ~75 types, which so far appear (at least in the case of PV6a3 Caligari and both AV1a1 neurons) to target multiple 4th order neurons. The decrease of non-unique parallel elements deeper in the brain is likely due to the fact that the first sensory layers need to deal with noisy signals from the external world, so a relatively large array of sensory neurons is needed. However, after signal averaging takes place in the AL, maintaining an equally large number of parallel neurons of the same type would be redundant, and energetically wasteful. The increase in number of unique elements on the other hand may reflect the increased demands of more complex, higher-order information processing. Work on the invertebrate visual system suggests that there is a similar trend taking place when moving from the retina to the brain [76]. However, it seems likely that the second trend (increase in unique parallel cell types) will reverse at some point, when moving deeper towards motor output: the number of DNs projecting to the nerve cord is estimated to be between 400-550 bilateral pairs [77,78], serving as a bottleneck before the actual motor responses that in the end make up the behavioural response of the animal. Secondly, although we observe a significant divergence of the geosmin pathway, the proportion of neurons receiving geosmin input changes relatively little from layer to layer: 25/1300=0.02 (ORNs), 5/150=0.03 (PNs), 131/1500=0.09 (LHNs) (Numbers are current estimates based on literature and EM data, and could still change for the LHNs. The LHN number includes everything with 1 or more connections from DA2 PNs, and setting a slightly higher threshold would decrease the proportion.). Thus, despite the observed divergence, geosmin is still encoded in a relatively sparse manner considering the LHN population as a whole.

Other animals, other sensory systems

Integration of similar or related sensory channels is likely to be a common computation occurring in nervous systems. In the highly streamlined nervous system of *C. elegans* this already takes place in the sensory neurons for olfactory information [79,80]. Here we have shown that in *Drosophila* the same process takes place slightly deeper in the brain: both at the axons of second order neurons, and in third order neurons. In rodents, the mitral cells (analogous to PNs in *Drosophila*) project from the olfactory bulb (analogous to the AL) into higher brain areas, such as entorhinal cortex, piriform cortex, amygdala and hypothalamus. Amygdala and hypothalamus are thought to be important for innate odour responses [4,81,82], and predator odours have been shown to activate similar areas of amygdala and hypothalamus [82], suggesting that there might be a similar convergence of innately aversive odour information. Regarding other sensory modalities, neurons preferentially responsive to complex stimuli such as faces [83,84], or vocalizations [85,86] seem likely to arise by similar circuit mechanisms; by integrating inputs from several simpler stimulus encoding neurons. The actual physiological integration properties of the LHNs described here remains an interesting open question. In principle, neurons such as the AV1a1 LHNs could fire strongly in response to activity of any of the input channels, in which case they perform a form of dimension reduction on the signal (where odour identities are lost, and replaced with a common denominator, such as *aversive*), or they could require the activity of multiple concurrent inputs. In the latter case, as AV1a1 neurons were also observed to receive input from food related odour channels, the activity of the neurons could actually encode a more complex *odour object,* such as the presence of a spoiled food source, rather than just the presence of aversive signals. In any case, arguably the first step in deciphering such higher olfactory computations for ecologically relevant olfactory stimuli is to find out which cells are involved, and how they connect and interact with each other. The results and approaches presented here take a significant step towards that goal.

Materials and Methods

Drosophila stocks and husbandry

The following stocks were used:

Canton S (UC San Diego Drosophila Stock Center, CA)
Ir8a^1; Ir25a^2; Orco^1, Gr63a^1(a kind gift from R. Benton)
w; Or56a-GAL4; + (Bloomington Drosophila Stock Center, Indiana)
w; MB247-GAL4; + (Bloomington Drosophila Stock Center, Indiana)
w; UAS-Kir2.1::GFP;+ (a kind gift from Matthias Landgraf)
w; +; R85E04 ([28], Bloomington Drosophila Stock Center, Indiana)
w; UAS-TNT-active form and w+; UAS-TNT-inactive form ([30], both kind gifts from C.O'Kane)
20XUAS-IVS-ChrimsonR::mVenus (Attp19);+;+ [87]
w; UAS-GCaMP3.0 (attP18);UAS-GCaMP3.0 (attP40)
w; UAS-mCD8::GFP; UAS-mCD8::GFP; +

The Split-GAL4 [88] lines for the optogenetic screen were made as a part of a larger collaborative screen for creating a cell-type specific driver line library for LHNs (details will be described in Dolan *et al.*, in preparation) by using a subset of the enhancer fragments used in making the original GMR GAL4 lines [28].

For most experiments flies were reared at 25°C and 60% humidity, under a 12:12 hour light-dark cycle, on food made with the following recipe: 4.8 l H_2O, 275 g of Glucose, 250 g yeast, 37 g agar, 175 g flour, 125 ml Nipagen solution, 50 ml penicillin/streptomycin, 20 ml propionic acid. The same food was used also for the egg-laying and female receptivity assays. For optogenetic behavioural experiments, flies were reared at 22□ on standard Iberian food containing yeast, cornmeal and agar, and supplemented with 1/500 all-trans retinal (Sigma-Aldrich, MO, USA).

Odour stimuli

Geosmin (CAS # 16423-19-1) was ordered from Sigma-Aldrich (Sigma-Aldrich, St. Louis, USA), Product Number UC18. Other odours (for **fig 1D** were same as used in [44]).

bioRxiv preprint doi: https://doi.org/10.1101/394403; this version posted August 26, 2018. The copyright holder for this preprint (which was not certified by peer review) is the author/funder, who has granted bioRxiv a license to display the preprint in perpetuity. It is made available under aCC-BY-NC 4.0 International license.

Behavioural assays

Egg-laying two-choice assay

Female flies were collected on the day of eclosion under CO2 anaesthesia, reared in same sex vials at 25oC and 60% humidity. Female flies aged 5-7 days were then mated with males of similar age for 6 hours on the day of the experiments. After six hours of mating the female flies were again isolated from the males under CO2 anaesthesia and were left to recover for 2 hours before starting the experiments. For the experiments, approximately 20 females were transferred without anaesthesia into a BugDorm insect rearing cage (24.5x24.5x24.5 cm) (MegaView Science Co., Ltd., TAIWAN) made of polyester netting. Two ø 50mm Petri dish plates containing Iberian fly food were placed in opposing corners of the cage and a small plastic cup cut from the cap of a 1.5 ml Eppendorf tube containing the experimental odour, or the solvent control, was placed at the center of each food plate. For the geosmin experiments either 5 or 50 µl of geosmin was used as a stimulus. For the experiments done with yeast odour, 100 µl of 400 mg/ml of baker's yeast in Milli-Q H2O was used. A nylon mesh was used for physically separating the flies from the odorant. All experiments started at 12:00 h Zeitgeber time (+/- 1 h) and lasted for 16 hours (+/- 1 h). Eggs were counted under a stereo microscope. An oviposition Preference Index (PI), was calculated by using the formula

$$PI = (Eggs\ on\ odour\ plate\ -\ Eggs\ on\ control\ plate) \div Eggs\ total$$

PI could thus get values from -1 to +1, signifying total avoidance and total preference of the geosmin plate, respectively.

Egg-laying no-choice assay

Fly collection, rearing and mating was performed similarly to the two-choice assay. For the no-choice assay, 5 females were aspirated without anaesthesia onto ø 50 mm Petri dish plates containing fly food, and the lid was placed on the plate. In the experiments where the effect of odorants on egg-laying quantity was tested, the stimuli were pipetted onto a small plastic cup cut from the cap of a 1.5 ml Eppendorf tube. 50 µl of geosmin was used as a stimulus. A nylon mesh was used for physically separating the flies from the odorant. All experiments started at 12:00 h Zeitgeber time (+/- 1 h) and lasted for 16 hours (+/- 1 h). Egg were counted under a stereo microscope.

Trap assay

Fly collection and rearing was performed similarly to the egg-laying assays. On day 5 half of the females were mated similarly to the egg-laying assays. After mating, 20 flies were placed in BugDorm insect rearing cages containing two conical flasks with attached pipette tips to facilitate entry and impede exit from the traps. Both flasks contained yeast mixed with H_2O (100 µl of 200 mg/ml of baker's yeast in Milli-Q H_2O) in order to attract the flies, and either geosmin (20ul of 1:1000) or mineral oil (20ul). All experiments started at 12:00 h Zeitgeber time (+/- 1 h) and lasted for 16 hours (+/- 1 h). The flies were counted in the morning and two variables were calculated: a PI (preference index) and Choice index:

$$PI = (Flies\ in\ the\ geosmin\ trap\ -\ Flies\ in\ the\ control\ trap) \div Total\ n\ of\ flies\ in\ traps$$

$$Choice\ Index = Total\ n\ of\ flies\ in\ traps \div Total\ n\ of\ flies$$

Female receptivity assay

Wild-type (Canton S) female virgin flies and anosmic mutant male (w; +; $Orco^1$ and $Ir8a^1$; $Ir25a^2$; $Orco^1$, $Gr63a^1$) flies were collected on the day of eclosion and isolated into same-sex vials (max 20-30 flies per vial) and used for experiments on day 6 or 7. Experiments were done on ø 35mm Petri dish plates filled with fly food. For the experiments testing the effects of odours on female receptivity, the odour delivery was performed similarly to the egg-laying assays. Experiments took place at 25°C in a temperature controlled incubator (Binder, Germany), under constant lighting, and lasted for 23 hours. Behaviour was imaged by using a Point Grey Chameleon camera, which was controlled via FView. The camera was set to take images once per minute. Mating behaviour was then scored manually and number of copulations (male mountings lasting for longer than 5 mins), latency to first mating, and time of matings were extracted as variables.

Male courtship assay

Canton S experimental males, and anosmic mutant (Ir8a1; Ir25a2; Orco1, Gr63a1) females were collected on the day of eclosion and isolated into same-sex vials. Flies were raised on regular Iberian food and were 5-7 days old when they were used for the experiments. Experiments took place in a perspex chamber apparatus consisting of 24 round courtship chambers (12 mm diameter, 5 mm height) and designed to fit on top of a 48 well-plate. Males and anosmic mutant females were aspirated into the chambers through sealable holes (3 mm diameter) unanaesthetised, and were kept separated from each other until the start of the experiment by a sliding metal partition. After being aspirated to the chambers flies were given 30 minutes to acclimatise to the chamber before starting the experiment. Either 20 µl of geosmin (1:1000), or mineral oil was pipetted into the wells of the 48 well-plate, and the plate was covered with nylon mesh, so that flies could smell the stimulus, but not be in contact with it. All experiments took place 05:00 (+/- 1) h Zeitgeber Time, and geosmin and control experiments were done on separate days, to avoid odour contamination. The chambers were washed with 70% ethanol and rinsed with running water after each experiment. Point Grey Chameleon camera controlled via FView was used for recording the experiments, and behaviour was scored manually.

Optogenetic four-field assay

The four-field optogenetic assay was carried out essentially as described Aso *et al. [17]*. Crosses were made on normal fly food containing 1:500 all-trans retinal (Sigma-Aldrich, MO, USA), and eclosed females of the right genotype were collected into same-sex vials under cold anaesthesia, and reared in the dark on 1:250 all-trans retinal food, at 22°C and 50% humidity. Approximately 20 female flies, aged 3-7 days were used for each experiment. The females were not specifically mated for the experiments, but they were producing fertilised eggs by the time of the experiments. The assay was performed on a circular arena of 10 cm diameter, and 3 mm height. Flies were transferred onto the arena without anaesthesia by using a vacuum pump. All experiments took place in darkness, at 25°C and 50% humidity. To prevent the infrared backlight from affecting the temperature in the arena, the arena was mounted on a heat sink, and an airflow of 150ml/min from the four corners of the arena to the centre was maintained.

A 617 nm wavelength LED (Red-Orange LUXEON Rebel LED; Luxeon Star LEDs, Brantford, Ontario, Canada) was used for the optical stimulation. The behaviour of the flies was recorded by using a camera (ROHS 1.3 MP B&W Flea3, US 3.0 Camera; Point Grey, Richmond, BC, Canada) equipped with a long-pass (800 nm) filter (B&W filter; Schneider Optics) set to capture at 30 Hz, and controlled

bioRxiv preprint doi: https://doi.org/10.1101/394403; this version posted August 26, 2018. The copyright holder for this preprint (which was not certified by peer review) is the author/funder, who has granted bioRxiv a license to display the preprint in perpetuity. It is made available under aCC-BY-NC 4.0 International license.

via a custom script written in Matlab. Only water was used for cleaning the arena.

Statistical analysis

All statistical analysis was performed with R. Shapiro-Wilk test was used for assessing normality of distributions. Normally distributed data was then analysed by using Welch's two-sample t-tests or Paired samples t-tests, whereas non-normally distributed data with Kruskal-Wallis rank sum tests, Wilcoxon rank sum tests, and Wilcoxon signed rank tests, where appropriate. Proportionality data was analysed with a Chi-squared test. For the egg-laying two-choice behavioural experiments (with R85E04 and LH728), power testing was done with effect size estimates based on data obtained on preliminary data on wild type and anosmic mutants (Ir8a[1]; Ir25a[2]; Orco[1], Gr63a[1]) (values used for power test estimates were wild type mean PI=-.45, SD=.6; anosmic mean PI=0, SD=.6, which gives an effect size estimate of Cohen's d=0.75), and based on this the required sample size for the experiments was 38.66, taking into account the Bonferroni corrected significance values. The power size estimations were done with the R package pwr.

Behavioural and imaging data throughout the paper are presented as notched box plots. The box represents the interquartile range of the sample (IQR, 25th - 75th percentiles) and is split by the median line. The whiskers extend to 1.5 x IQR beyond the box and the notches represent the 95% confidence interval for the sample median. The points mark individual sample points and asymmetrical notches indicate skewed distributions.

Immunohistochemistry

Immunohistochemistry with antibodies was done similarly to [20], and the chemical labelling similarly to [89], with the exception of an overnight blocking step being used for antibody stainings. Primary antibodies used were: 1:20 mouse anti-nc82 (DSHB, University of Iowa, USA), 1:1600 chicken anti-GFP (ab13970, Abcam, Cambridge, UK), 1:200 rabbit anti-GABA (A2052, Sigma-Aldrich, MO, USA), and 1:400 mouse anti-ChAT (4B1, DSHB, University of Iowa, USA). Secondary antibodies were: Alexa-488 Goat anti-chicken, Alexa-568 Goat anti-Rabbit, Goat anti-mouse 633, all 1:800 (Life Technologies, Carlsbad, CA). For the chemical labelling, 1:1000 concentrations of SNAP-Surface 488 (NEB #S9124, New England Biolabs, Ipswich, MA), TMR Halo (G8252, Promega, Madison, WI) were used. Finally, brains were mounted on charged slides (Menzel- Gläser, Braunschweig, Germany) using Vectashield (Vector Laboratories) as the mounting medium.

Confocal microscopy

A Zeiss 710 confocal microscope was used for image acquisition. Brains were imaged at 768 x 768, or 2048x1024 (AL closeup), pixel resolution in 1 mm slices (voxel size: (0.46 x 0.46 x 1 mm) using an EC Plan-Neofluar 40x/1.30 oil immersion objective (Carl Zeiss AG, Jena, Germany) and 0.6 zoom factor. All images were acquired at 16 bit colour depth.

Image processing and analysis

Image registration

Image registration for the confocal data was as carried out according to [90]. In brief: the presynaptic marker Bruchpilot (here labelled by nc82 or Brp-SNAP) was used as a basis for performing an intensity-based non-linear warping registration onto a template brain (JFRC2 or JFRC2013). The registration procedure itself was performed by using the cross platform Computational Morphometry Tool Kit software (http://www.nitrc.org/projects/cmtk). Bridging registrations were used for transforming neurons from one template brain to another [39,91] by using the nat.flybrains (http://jefferislab.github.io/nat.flybrains, 10.5281/zenodo.1401049) R package.

Light-level neuron tracing

Registered confocal images were either obtained de novo (for comparing LH1983 to EM skeletons) or from Costa *et al.* [32] based on original raw data from the FlyCircuit dataset available at flycircuit.tw [31], for comparing PN morphologies. 3D reconstructions of neurons were then created by using semi-automated tracing in Amira software (Zuse Institute, Berlin, Germany) using the hxskeletonize plugin [31,92]. 3D reconstructions for DL5 and VA7l were obtained from [20].

EM tracing

Neuron skeletons were manually traced in a full adult *Drosophila* EM volume [39] using CATMAID [40,41]. PN glomeruli had been identified earlier by [39] for the right side of the brain. PNs on the left side of the brain were identified in the same way, and selected left-right pairs of glomeruli were confirmed by identifying the ORNs providing input to the PNs in the right AL and tracing them across the brain to the left AL.

Potential DA2 axo-axonic connectivity

To assess whether or not the DA2-DL4 connectivity was specific, we checked which PN skeletons pass within 1µm of a DA2 output synapse in the LH. (In the right LH, approximately 86% of PN-PN axo-axonic synapses occur within this threshold.) Each instance where a PN skeleton was within this 1µm radius was counted as a single potential synapse. This potential connectivity was then compared to the actual axo-axonic connectivity of the DA2 PNs.

EM downstream sampling

We used a random sampling approach to identify neurons downstream of DA2 PNs in the LH. Identified DA2 PNs (as well as all other uniglomerular PNs in the medial (mALT) and mediolateral (mlALT) antennal lobe tract) were completely reconstructed within the LH. Synapses were identified, and all postsynaptic nodes were annotated for each (consistent with the criteria described in [21]). Once completed, the full set of postsynaptic nodes for a single representative DA2 PN was randomised. Each postsynaptic node was then used as a starting point for tracing out a downstream partner. If a postsynaptic node could not be connected to a neuronal backbone (defined by the presence of visible microtubules) as a result of ambiguous features or missing sections, it was excluded from further analysis. Approximately 20% of postsynaptic nodes (not counting those excluded on the criteria above) were sampled in this way; this number was deemed sufficient to identify the most strongly-connected neurons downstream of the DA2 PNs, based on the increasing frequency of starting nodes being connected to previously identified neurons (**fig S2D**). This basic sampling procedure was repeated for the axons of selected third order neurons (AV1a1 Duck and PV6a3 Caligari).

Partner neurons were initially traced just enough to identify a soma, thus confirming whether the starting node belonged to a unique or previously traced neuron. LHNs of particular interest (PV6a3 Caligari, AV1a1 Duck and Pigeon) were then traced to completion; all identifiable branches of the neuron were fully traced, and all incoming and outgoing synapses annotated. With tracing completed, we were able to examine these neurons' complete morphology (manually identifying

bioRxiv preprint doi: https://doi.org/10.1101/394403; this version posted August 26, 2018. The copyright holder for this preprint (which was not certified by peer review) is the author/funder, who has granted bioRxiv a license to display the preprint in perpetuity. It is made available under aCC-BY-NC 4.0 International license.

the primary neurite, dendrites, and axon for each), as well as their PN inputs within the LH.
While we only sampled from one of the five DA2 PNs on the right side of the brain, our data suggest that the more strongly-connected downstream partners should be consistent across all PNs in the group. In general, the number of times a neuron was hit in our sample correlates with the number of DA2 PNs it receives input from. Additionally, looking at five LHNs identified in our sample that were traced to completion (and thus have all their PN input identified) shows a clear correlation between total number of DA2 inputs and the number of upstream DA2 PNs.

Light versus EM comparisons of neuron morphology

All neurons taking the AV1 tract were traced far enough to identify major branches and overall morphology in the EM volume. The light-level tracing of AV1a1 was obtained from LH1983. Both light and EM neurons were converted to the FCWB reference space via nat.flybrains and elmr (https://github.com/jefferis/elmr, 10.5281/zenodo.1401050) R packages. elmr uses landmarks generated using the Fiji elm plugin (https://github.com/saalfeldlab/elm). The primary neurite tract was then removed from the neurons for analysis, and the light-level tracing was compared to all the EM tracings from the AV tract by using the NBLAST algorithm [32].

Clustering of neuron morphology

Neurons downstream of DA2 PNs were converted to *dot properties* representations [32,93] using the nat.nblast package (https://github.com/jefferislab/nat.nblast) [32]). The NBLAST algorithm [32] was then used to generate an all by all similarity matrix. Hierarchical clustering was performed on the resulting distance matrix using the Ward's method (via hclust function). Cut height for the clustering was set to 0.8, after manually assessing the cluster groups.

In silico anatomy screen

For the *in silico* anatomical screen, the Segmentation Editor tool in the Fiji software (NIH, Bethesda, USA) was used to create binary masks of the DA2 PNs. Masked neurons were them maximum projected and merged with JFRC2 template brain [28]. Janelia FlyLight GAL4 lines [28] with expression patterns in the LH were then loaded into the same template brain with the mask in order to visually look for driver lines and neuronal clusters with overlap with the DA2 PNs. Each line was then scored for goodness of overlap, and neurons for the best matches were identified based on earlier annotation work of LH neurons done in the lab [44], and then cross-identified in LH Split-GAL4 lines (Dolan *et al.*, in preparation).

Neuronal morphology nomenclature

Annotation of neuronal types was based on Frechter *et al.* [44] (for LHNs) and Namiki *et al.* [77] (for DNs). Image data for light level type example skeletons from FlyCircuit can be browsed by searching for the neuron identifier at http://www.virtualflybrain.org/.

Electrophysiology

In vivo patch-clamp recordings from the DA2 projection neurons were carried out as described in [44] using the R85E04 driver line and mCD8::GFP to label the neurons. Analysis of recordings used the open source gphys R (CRAN, http://www.r-project.org) package (see http://jefferis.github.io/gphys).

In vivo calcium imaging

Functional imaging experiments on AV1a1 neurons were performed on flies containing two copies of UAS-GCaMP3 (at attP18 and attP40) driven by LH728 Split-GAL4 driver. GCaMP3 was used instead of newer versions of GCaMP for its higher baseline fluorescence which allowed easier identification of the neurons. Flies were placed into custom built holders, leaving the head and thorax exposed, under CO_2 anaesthesia and secured in place with UV curable glue (Kemxert, KOA 300). Wax was used for securing the legs and the proboscis. A window was then cut into the head capsule with sharp forceps, and trachea and air sacks were removed in order to uncover the brain. Fly brains were bathed in external saline ([94], see table below) adjusted to 275mM and 7.3 pH, and bubbled with 5% CO_2. The antennae were left under the holder so that they could be exposed to odour stimuli.
A custom-built setup based on the Sutter (Novato, CA) Movable Objective Microscope with a Zeiss W Plan-Apochromat 20x/1.0 objective was used for the two photon imaging. A Coherent (Santa Clara, CA) Chameleon Vision Ti-Sapphire provided excitation, and image acquisition was controlled by ScanImage software [95]. Image acquisition and odour delivery were triggered by a separate PC running Igor Pro software (Wavemetrics, Lake Oswego, OR) running Neuromatic. Images were captured at 8Hz at 265x255 pixel, and two photon excitation was provided at 900 nm. Odour stimulation was performed largely similarly to [23]. Odour delivery started at 3000 ms after the beginning of a trial and lasted for 2000 ms. Image analysis was performed with custom scripts written in R employing the open source scanimage package (see https://github.com/jefferis/scanimage, 10.5281/zenodo.1401028). Data was both manually checked for motion artifacts, and excluded from analysis if there were larger than 5% dF/F peaks during the baseline recording epoch, or if there were not larger than 5% dF/F responses to any of the tested odours during the stimulation epoch.

	Concentration (mM)
NaCl	104.75
KCl	5
NaH_2PO_4	1
$MgCL_2.6H_2O$	1
$CaCl_2.2H_2O$	1
$NaHCO_3$	26
TES	5
glucose	10
trehalose	10

bioRxiv preprint doi: https://doi.org/10.1101/394403; this version posted August 26, 2018. The copyright holder for this preprint (which was not certified by peer review) is the author/funder, who has granted bioRxiv a license to display the preprint in perpetuity. It is made available under aCC-BY-NC 4.0 International license.

Acknowledgements

We thank Richard Benton, Matthias Landgraf, and Cahir O'Kane, as well as the Bloomington and UC San Diego stock centres for fly stocks. We thank Johann Schor, Joe Hsu, Amelia Edmondson-Stait, Adam Heath, Nadiya Sharifi, Serene Dhawan, Lindsey Tagg, Mahmoud Elbahnasawi, Ali Jawaid Iqabal, Lucia Kmecova, Remy Tabano, Elizabeth Marin and Fei Wang for additional EM tracing, and Scott Lauritzen for tracing supervision and training. Images from FlyCircuit were obtained from the NCHC (National Center for High-performance Computing) and NTHU (National Tsing Hua University), Hsinchu, Taiwan. We would also like to thank the Finkelstein Lab for sharing an easy to use Biorxiv template (https://github.com/finkelsteinlab/BioRxiv-Template).

This work was supported by an ERC Consolidator grant (649111) and core support from the MRC (MC-U105188491) (to G.S.X.E.J.) and a Wellcome Trust Collaborative Award (203261/Z/16/Z to G.S.X.E.J., D.B., G.M.R.). Generation of split GAL4 lines was supported by the Janelia Visiting Scientist Program. P.H. was supported by an MRC LMB PhD Studentship and Cambridge Home and EU Scholarship Scheme stipend, M-J.D. by an MRC LMB, Boehringer Ingelheim Fonds and Janelia Graduate Research Fellowships, Z.M. by an Amgen summer studentship. The authors declare no conflict of interest.

References

1. Su, C.-Y., Menuz, K., and Carlson, J.R. (2009). Olfactory perception: receptors, cells, and circuits. Cell *139*, 45–59.
2. de Belle, J.S., and Heisenberg, M. (1994). Associative odor learning in Drosophila abolished by chemical ablation of mushroom bodies. Science *263*, 692–695.
3. Choi, G.B., Stettler, D.D., Kallman, B.R., Bhaskar, S.T., Fleischmann, A., and Axel, R. (2011). Driving opposing behaviors with ensembles of piriform neurons. Cell *146*, 1004–1015.
4. Root, C.M., Denny, C.A., Hen, R., and Axel, R. (2014). The participation of cortical amygdala in innate, odour-driven behaviour. Nature *515*, 269–273.
5. Masse, N.Y., Turner, G.C., and Jefferis, G.S.X.E. (2009). Olfactory Information Processing in Drosophila. Curr. Biol. *19*, R700–R713.
6. Wilson, R.I. (2013). Early olfactory processing in Drosophila: mechanisms and principles. Annu. Rev. Neurosci. *36*, 217–241.
7. Couto, A., Alenius, M., and Dickson, B.J. (2005). Molecular, anatomical, and functional organization of the Drosophila olfactory system. Curr. Biol. *15*, 1535–1547.
8. Fishilevich, E., and Vosshall, L.B. (2007). Genetic and Functional Subdivision of the Drosophila Antennal Lobe. Curr. Biol. *17*, 1180.
9. Hallem, E.A., and Carlson, J.R. (2006). Coding of odors by a receptor repertoire. Cell *125*, 143–160.
10. Jones, W.D., Cayirlioglu, P., Kadow, I.G., and Vosshall, L.B. (2006). Two chemosensory receptors together mediate carbon dioxide detection in Drosophila. Nature *445*, 86–90.
11. van der Goes van Naters, W., and Carlson, J.R. (2007). Receptors and Neurons for Fly Odors in Drosophila. Curr. Biol. *17*, 606–612.
12. Stensmyr, M.C., Dweck, H.K.M., Farhan, A., Ibba, I., Strutz, A., Mukunda, L., Linz, J., Grabe, V., Steck, K., Lavista-Llanos, S., *et al.* (2012). A conserved dedicated olfactory circuit for detecting harmful microbes in Drosophila. Cell *151*, 1345–1357.
13. Vosshall, L.B., Wong, A.M., and Axel, R. (2000). An olfactory sensory map in the fly brain. Cell *102*, 147–159.
14. Grabe, V., Baschwitz, A., Dweck, H.K.M., Lavista-Llanos, S., Hansson, B.S., and Sachse, S. (2016). Elucidating the Neuronal Architecture of Olfactory Glomeruli in the Drosophila Antennal Lobe. Cell Rep. *16*, 3401–3413.
15. Caron, S.J.C., Ruta, V., Abbott, L.F., and Axel, R. (2013). Random convergence of olfactory inputs in the Drosophila mushroom body. Nature *497*, 113–117.
16. Aso, Y., Hattori, D., Yu, Y., Johnston, R.M., Iyer, N.A., Ngo, T.-T.B., Dionne, H., Abbott, L.F., Axel, R., Tanimoto, H., *et al.* (2014). The neuronal architecture of the mushroom body provides a logic for associative learning. Elife *3*, e04577.
17. Aso, Y., Sitaraman, D., Ichinose, T., Kaun, K.R., Vogt, K., Belliart-Guérin, G., Plaçais, P.-Y., Robie, A.A., Yamagata, N., Schnaitmann, C., *et al.* (2014). Mushroom body output neurons encode valence and guide memory-based action selection in Drosophila. Elife *3*, e04580.
18. Hige, T., Aso, Y., Modi, M.N., Rubin, G.M., and Turner, G.C. (2015). Heterosynaptic Plasticity Underlies Aversive Olfactory Learning in Drosophila. Neuron *88*, 985–998.
19. Heimbeck, G., Bugnon, V., Gendre, N., Keller, A., and Stocker, R.F. (2001). A central neural circuit for experience-independent olfactory and courtship behavior in Drosophila melanogaster. Proc. Natl. Acad. Sci. U. S. A. *98*, 15336–15341.
20. Jefferis, G.S.X.E., Potter, C.J., Chan, A.M., Marin, E.C., Rohlfing, T., Maurer, C.R., Jr, and Luo, L. (2007). Comprehensive maps of Drosophila higher olfactory centers: spatially segregated fruit and pheromone representation. Cell *128*, 1187–1203.
21. Datta, S.R., Vasconcelos, M.L., Ruta, V., Luo, S., Wong, A., Demir, E., Flores, J., Balonze, K., Dickson, B.J., and Axel, R. (2008). The Drosophila pheromone cVA activates a sexually dimorphic neural circuit. Nature *452*, 473–477.
22. Ruta, V., Datta, S.R., Vasconcelos, M.L., Freeland, J., Looger, L.L., and Axel, R. (2010). A dimorphic pheromone circuit in Drosophila from sensory input to descending output. Nature *468*, 686–690.
23. Kohl, J., Ostrovsky, A.D., Frechter, S., and Jefferis, G.S.X.E. (2013). A bidirectional circuit switch reroutes pheromone signals in male and female brains. Cell *155*, 1610–1623.
24. Steck, K., Veit, D., Grandy, R., Badia, S.B. i., Mathews, Z., Verschure, P., Hansson, B.S., and Knaden, M. (2012). A high-throughput behavioral paradigm for Drosophila olfaction - The Flywalk. Sci. Rep. *2*. Available at: http://dx.doi.org/10.1038/srep00361.
25. van Breugel, F., Huda, A., and Dickinson, M.H. (2017). Drosophila have distinct activity-gated pathways that mediate attraction and aversion to CO2. Available at: http://dx.doi.org/10.1101/227991.
26. Christensen, T.A., and Hildebrand, J.G. (1987). Male-specific, sex pheromone-selective projection neurons in the antennal lobes of the moth Manduca sexta. J. Comp. Physiol. A *160*, 553–569.
27. Schlief, M.L., and Wilson, R.I. (2007). Olfactory processing and behavior downstream from highly selective receptor neurons. Nat. Neurosci. *10*, 623–630.
28. Jenett, A., Rubin, G.M., Ngo, T.-T.B., Shepherd, D., Murphy, C., Dionne, H., Pfeiffer, B.D., Cavallaro, A., Hall, D., Jeter, J., *et al.* (2012). A GAL4-driver line resource for Drosophila neurobiology. Cell Rep. *2*, 991–1001.
29. Kohl, J., Ng, J., Cachero, S., Dolan, M.-J., Sutcliffe, B., Krüger, D., Frechter, S., and Jefferis, G.S. (2014). Ultra fast tissue staining with chemical tags. Available at: http://dx.doi.org/10.1101/005298.
30. Sweeney, S.T., Broadie, K., Keane, J., Niemann, H., and O'Kane, C.J. (1995). Targeted expression of tetanus toxin light chain in Drosophila specifically eliminates synaptic transmission and causes behavioral defects. Neuron *14*, 341–351.
31. Chiang, A.-S., Lin, C.-Y., Chuang, C.-C., Chang, H.-M., Hsieh, C.-H., Yeh, C.-W., Shih, C.-T., Wu, J.-J., Wang, G.-T., Chen, Y.-C., *et al.* (2011). Three-dimensional reconstruction of brain-wide wiring networks in Drosophila at single-cell resolution. Curr. Biol. *21*, 1–11.
32. Costa, M., Manton, J.D., Ostrovsky, A.D., Prohaska, S., and Jefferis, G.S.X.E. (2016). NBLAST: Rapid, Sensitive Comparison of

bioRxiv preprint doi: https://doi.org/10.1101/394403; this version posted August 26, 2018. The copyright holder for this preprint (which was not certified by peer review) is the author/funder, who has granted bioRxiv a license to display the preprint in perpetuity. It is made available under aCC-BY-NC 4.0 International license.

Neuronal Structure and Construction of Neuron Family Databases. Neuron *91*, 293–311.

33. Ebrahim, S.A.M., Dweck, H.K.M., Stökl, J., Hofferberth, J.E., Trona, F., Weniger, K., Rybak, J., Seki, Y., Stensmyr, M.C., Sachse, S., *et al.* (2015). Drosophila Avoids Parasitoids by Sensing Their Semiochemicals via a Dedicated Olfactory Circuit. PLoS Biol. *13*, e1002318.
34. Suh, G.S.B., Wong, A.M., Hergarden, A.C., Wang, J.W., Simon, A.F., Benzer, S., Axel, R., and Anderson, D.J. (2004). A single population of olfactory sensory neurons mediates an innate avoidance behaviour in Drosophila. Nature *431*, 854–859.
35. Knaden, M., Strutz, A., Ahsan, J., Sachse, S., and Hansson, B.S. (2012). Spatial Representation of Odorant Valence in an Insect Brain. Cell Rep. *1*, 392–399.
36. Mansourian, S., Corcoran, J., Enjin, A., Löfstedt, C., Dacke, M., and Stensmyr, M.C. (2016). Fecal-Derived Phenol Induces Egg-Laying Aversion in Drosophila. Curr. Biol. *26*, 2762–2769.
37. Min, S., Ai, M., Shin, S.A., and Suh, G.S.B. (2013). Dedicated olfactory neurons mediating attraction behavior to ammonia and amines in Drosophila. Proc. Natl. Acad. Sci. U. S. A. *110*, E1321–9.
38. Chin, S.G., Maguire, S.E., Huoviala, P., Gregory S X, and Potter, C.J. (2017). An olfactogenetic approach identifies olfactory neurons and brain centers directing negative oviposition decisions in Drosophila. Available at: http://dx.doi.org/10.1101/206342.
39. Zheng, Z., Lauritzen, J.S., Perlman, E., Robinson, C.G., Nichols, M., Milkie, D., Torrens, O., Price, J., Fisher, C.B., Sharifi, N., *et al.* (2018). A Complete Electron Microscopy Volume of the Brain of Adult Drosophila melanogaster. Cell. Available at: http://dx.doi.org/10.1016/j.cell.2018.06.019.
40. Schneider-Mizell, C.M., Gerhard, S., Longair, M., Kazimiers, T., Li, F., Zwart, M.F., Champion, A., Midgley, F.M., Fetter, R.D., Saalfeld, S., *et al.* (2016). Quantitative neuroanatomy for connectomics in Drosophila. Elife *5*. Available at: http://dx.doi.org/10.7554/eLife.12059.
41. Saalfeld, S., Cardona, A., Hartenstein, V., and Tomancak, P. (2009). CATMAID: collaborative annotation toolkit for massive amounts of image data. Bioinformatics *25*, 1984–1986.
42. Jeanne, J.M., and Wilson, R.I. (2015). Convergence, Divergence, and Reconvergence in a Feedforward Network Improves Neural Speed and Accuracy. Neuron *88*, 1014–1026.
43. Frank, D.D., Enjin, A., Jouandet, G.C., Zaharieva, E.E., Para, A., Stensmyr, M.C., and Gallio, M. (2017). Early Integration of Temperature and Humidity Stimuli in the Drosophila Brain. Curr. Biol. *27*, 2381–2388.e4.
44. Frechter, S., Bates, A.S., Tootoonian, S., Dolan, M.-J., Manton, J.D., Jamasb, A., Kohl, J., Bock, D., and Jefferis, G.S.X.E. (2018). Functional and Anatomical Specificity in a Higher Olfactory Centre. Available at: http://dx.doi.org/10.1101/336982.
45. Ito, K., Shinomiya, K., Ito, M., Armstrong, J.D., Boyan, G., Hartenstein, V., Harzsch, S., Heisenberg, M., Homberg, U., Jenett, A., *et al.* (2014). A systematic nomenclature for the insect brain. Neuron *81*, 755–765.
46. Kamikouchi, A., Shimada, T., and Ito, K. (2006). Comprehensive classification of the auditory sensory projections in the brain of the fruit flyDrosophila melanogaster. J. Comp. Neurol. *499*, 317–356.
47. Miyamoto, T., and Amrein, H. (2008). Suppression of male courtship by a Drosophila pheromone receptor. Nat. Neurosci. *11*, 874–876.
48. Clowney, E.J., Iguchi, S., Bussell, J.J., Scheer, E., and Ruta, V. (2015). Multimodal Chemosensory Circuits Controlling Male Courtship in Drosophila. Neuron *87*, 1036–1049.
49. Shih, C.-T., Sporns, O., Yuan, S.-L., Su, T.-S., Lin, Y.-J., Chuang, C.-C., Wang, T.-Y., Lo, C.-C., Greenspan, R.J., and Chiang, A.-S. (2015). Connectomics-based analysis of information flow in the Drosophila brain. Curr. Biol. *25*, 1249–1258.
50. Jeanne, J.M., Fişek, M., and Wilson, R.I. (2018). The Organization of Projections from Olfactory Glomeruli onto Higher-Order Neurons. Neuron *98*, 1198–1213.e6.
51. Münch, D., and Giovanni Galizia, C. (2016). DoOR 2.0 - Comprehensive Mapping of Drosophila melanogaster Odorant Responses. Sci. Rep. *6*. Available at: http://dx.doi.org/10.1038/srep21841.
52. Ai, M., Min, S., Grosjean, Y., Leblanc, C., Bell, R., Benton, R., and Suh, G.S.B. (2010). Acid sensing by the Drosophila olfactory system. Nature *468*, 691–695.
53. Jiang, H., Lkhagva, A., Daubnerová, I., Chae, H.-S., Šimo, L., Jung, S.-H., Yoon, Y.-K., Lee, N.-R., Seong, J.Y., Žitňan, D., *et al.* (2013). Natalisin, a tachykinin-like signaling system, regulates sexual activity and fecundity in insects. Proc. Natl. Acad. Sci. U. S. A. *110*, E3526–34.
54. Mansourian, S., and Stensmyr, M.C. (2015). The chemical ecology of the fly. Curr. Opin. Neurobiol. *34*, 95–102.
55. Dweck, H.K.M., Ebrahim, S.A.M., Thoma, M., Mohamed, A.A.M., Keesey, I.W., Trona, F., Lavista-Llanos, S., Svatoš, A., Sachse, S., Knaden, M., *et al.* (2015). Pheromones mediating copulation and attraction in Drosophila. Proc. Natl. Acad. Sci. U. S. A. *112*, E2829–35.
56. Silbering, A.F., Rytz, R., Grosjean, Y., Abuin, L., Ramdya, P., Jefferis, G.S.X.E., and Benton, R. (2011). Complementary function and integrated wiring of the evolutionarily distinct Drosophila olfactory subsystems. J. Neurosci. *31*, 13357–13375.
57. Rimal, S., and Lee, Y. (2018). The multidimensional ionotropic receptors of Drosophila melanogaster. Insect Mol. Biol. *27*, 1–7.
58. Hussain, A., Zhang, M., Üçpunar, H.K., Svensson, T., Quillery, E., Gompel, N., Ignell, R., and Grunwald Kadow, I.C. (2016). Ionotropic Chemosensory Receptors Mediate the Taste and Smell of Polyamines. PLoS Biol. *14*, e1002454.
59. Strutz, A., Soelter, J., Baschwitz, A., Farhan, A., Grabe, V., Rybak, J., Knaden, M., Schmuker, M., Hansson, B.S., and Sachse, S. (2014). Decoding odor quality and intensity in the Drosophila brain. Elife *3*. Available at: http://dx.doi.org/10.7554/elife.04147.
60. Tian, L., Hires, S.A., Mao, T., Huber, D., Chiappe, M.E., Chalasani, S.H., Petreanu, L., Akerboom, J., McKinney, S.A., Schreiter, E.R., *et al.* (2009). Imaging neural activity in worms, flies and mice with improved GCaMP calcium indicators. Nat. Methods *6*, 875–881.
61. Marin, E.C., Watts, R.J., Tanaka, N.K., Ito, K., and Luo, L. (2005). Developmentally programmed remodeling of the Drosophila olfactory circuit. Development *132*, 725–737.
62. Lin, S., Kao, C.-F., Yu, H.-H., Huang, Y., and Lee, T. (2012). Lineage analysis of Drosophila lateral antennal lobe neurons reveals notch-dependent binary temporal fate decisions. PLoS Biol. *10*, e1001425.
63. Attwell, D., and Laughlin, S.B. (2001). An energy budget for signaling in the grey matter of the brain. J. Cereb. Blood Flow Metab. *21*, 1133–1145.
64. Harris, J.J., Jolivet, R., and Attwell, D. (2012). Synaptic Energy Use and Supply. Neuron *75*, 762–777.
65. Niven, J.E., Anderson, J.C., and Laughlin, S.B. (2007). Fly photoreceptors demonstrate energy-information trade-offs in neural coding. PLoS Biol. *5*, e116.
66. Niven, J.E., and Laughlin, S.B. (2008). Energy limitation as a selective pressure on the evolution of sensory systems. J. Exp. Biol. *211*, 1792–1804.
67. Grosjean, Y., Rytz, R., Farine, J.-P., Abuin, L., Cortot, J., Jefferis, G.S.X.E., and Benton, R. (2011). An olfactory receptor for food-derived odours promotes male courtship in Drosophila. Nature *478*, 236–240.

bioRxiv preprint doi: https://doi.org/10.1101/394403; this version posted August 26, 2018. The copyright holder for this preprint (which was not certified by peer review) is the author/funder, who has granted bioRxiv a license to display the preprint in perpetuity. It is made available under aCC-BY-NC 4.0 International license.

68. Bell, J.S., and Wilson, R.I. (2016). Behavior Reveals Selective Summation and Max Pooling among Olfactory Processing Channels. Neuron *91*, 425–438.
69. Álvarez-Salvado, E., Licata, A., Connor, E.G., McHugh, M.K., King, B.M.N., Stavropoulos, N., Crimaldi, J.P., and Nagel, K.I. (2018). Elementary sensory-motor transformations underlying olfactory navigation in walking fruit-flies. Available at: http://dx.doi.org/10.1101/307660.
70. Root, C.M., Ko, K.I., Jafari, A., and Wang, J.W. (2011). Presynaptic facilitation by neuropeptide signaling mediates odor-driven food search. Cell *145*, 133–144.
71. Quinn, W.G., Harris, W.A., and Benzer, S. (1974). Conditioned Behavior in Drosophila melanogaster. Proceedings of the National Academy of Sciences *71*, 708–712.
72. Keene, A.C., and Waddell, S. (2007). Drosophila olfactory memory: single genes to complex neural circuits. Nat. Rev. Neurosci. *8*, 341–354.
73. Gao, X.J., Potter, C.J., Gohl, D.M., Silies, M., Katsov, A.Y., Clandinin, T.R., and Luo, L. (2013). Specific kinematics and motor-related neurons for aversive chemotaxis in Drosophila. Curr. Biol. *23*, 1163–1172.
74. Jung, S.-H., Hueston, C., and Bhandawat, V. (2015). Odor-identity dependent motor programs underlie behavioral responses to odors. Elife *4*. Available at: http://dx.doi.org/10.7554/eLife.11092.
75. von Reyn, C.R., Nern, A., Williamson, W.R., Breads, P., Wu, M., Namiki, S., and Card, G.M. (2017). Feature Integration Drives Probabilistic Behavior in the Drosophila Escape Response. Neuron *94*, 1190–1204.e6.
76. Robles, E., Laurell, E., and Baier, H. (2014). The retinal projectome reveals brain-area-specific visual representations generated by ganglion cell diversity. Curr. Biol. *24*, 2085–2096.
77. Namiki, S., Dickinson, M.H., Wong, A.M., Korff, W., and Card, G.M. (2017). The functional organization of descending sensory-motor pathways in Drosophila. Available at: http://dx.doi.org/10.1101/231696.
78. Hsu, C.T., and Bhandawat, V. (2016). Organization of descending neurons in Drosophila melanogaster. Sci. Rep. *6*, 20259.
79. Bargmann, C.I., Hartwieg, E., and Robert Horvitz, H. (1993). Odorant-selective genes and neurons mediate olfaction in C. elegans. Cell *74*, 515–527.
80. Troemel, E.R., Kimmel, B.E., and Bargmann, C.I. (1997). Reprogramming Chemotaxis Responses: Sensory Neurons Define Olfactory Preferences in C. elegans. Cell *91*, 161–169.
81. Motta, S.C., Goto, M., Gouveia, F.V., Baldo, M.V.C., Canteras, N.S., and Swanson, L.W. (2009). Dissecting the brain's fear system reveals the hypothalamus is critical for responding in subordinate conspecific intruders. Proceedings of the National Academy of Sciences *106*, 4870–4875.
82. Pérez-Gómez, A., Bleymehl, K., Stein, B., Pyrski, M., Birnbaumer, L., Munger, S.D., Leinders-Zufall, T., Zufall, F., and Chamero, P. (2015). Innate Predator Odor Aversion Driven by Parallel Olfactory Subsystems that Converge in the Ventromedial Hypothalamus. Curr. Biol. *25*, 1340–1346.
83. Perrett, D.I., Rolls, E.T., and Caan, W. (1982). Visual neurones responsive to faces in the monkey temporal cortex. Exp. Brain Res. *47*, 329–342.
84. Tsao, D.Y., Freiwald, W.A., Tootell, R.B.H., and Livingstone, M.S. (2006). A cortical region consisting entirely of face-selective cells. Science *311*, 670–674.
85. Rauschecker, J.P., Tian, B., and Hauser, M. (1995). Processing of complex sounds in the macaque nonprimary auditory cortex. Science *268*, 111–114.
86. Romanski, L.M., and Goldman-Rakic, P.S. (2001). An auditory domain in primate prefrontal cortex. Nat. Neurosci. *5*, 15–16.
87. Klapoetke, N.C., Murata, Y., Kim, S.S., Pulver, S.R., Birdsey-Benson, A., Cho, Y.K., Morimoto, T.K., Chuong, A.S., Carpenter, E.J., Tian, Z., *et al.* (2014). Independent optical excitation of distinct neural populations. Nat. Methods *11*, 338–346.
88. Luan, H., Peabody, N.C., Vinson, C.R., and White, B.H. (2006). Refined Spatial Manipulation of Neuronal Function by Combinatorial Restriction of Transgene Expression. Neuron *52*, 425–436.
89. Kohl, J., Ng, J., Cachero, S., Ciabatti, E., Dolan, M.-J., Sutcliffe, B., Tozer, A., Ruehle, S., Krueger, D., Frechter, S., *et al.* (2014). Ultrafast tissue staining with chemical tags. Proc. Natl. Acad. Sci. U. S. A. *111*, E3805–14.
90. Cachero, S., Ostrovsky, A.D., Yu, J.Y., Dickson, B.J., and Jefferis, G.S.X.E. (2010). Sexual dimorphism in the fly brain. Curr. Biol. *20*, 1589–1601.
91. Manton, J.D., Ostrovsky, A.D., Goetz, L., Costa, M., Rohlfing, T., and Gregory S X (2014). Combining genome-scale Drosophila 3D neuroanatomical data by bridging template brains. Available at: http://dx.doi.org/10.1101/006353.
92. Evers, J.F., Schmitt, S., Sibila, M., and Duch, C. (2005). Progress in Functional Neuroanatomy: Precise Automatic Geometric Reconstruction of Neuronal Morphology From Confocal Image Stacks. J. Neurophysiol. *93*, 2331–2342.
93. Masse, N.Y., Cachero, S., Ostrovsky, A.D., and Jefferis, G.S.X.E. (2012). A mutual information approach to automate identification of neuronal clusters in Drosophila brain images. Front. Neuroinform. *6*, 21.
94. Wilson, R.I., Turner, G.C., and Laurent, G. (2004). Transformation of olfactory representations in the Drosophila antennal lobe. Science *303*, 366–370.
95. Pologruto, T.A., Sabatini, B.L., and Svoboda, K. (2003). ScanImage: flexible software for operating laser scanning microscopes. Biomed. Eng. Online *2*, 13.

bioRxiv preprint doi: https://doi.org/10.1101/394403; this version posted August 26, 2018. The copyright holder for this preprint (which was not certified by peer review) is the author/funder, who has granted bioRxiv a license to display the preprint in perpetuity. It is made available under aCC-BY-NC 4.0 International license.

Supplementary Figures

Figure S1: Supplementary data 1

(A) A maximum intensity projection of a Or56a-GAL4 confocal stack. Green channel marks the GFP, and magenta the nc82 neuropil stain.
(B) Egg-laying two-choice preference indices (PI) to geosmin for wild type (Canton S) flies, with two different stimulus quantities. Wilcoxon signed rank test with continuity correction for testing the values against 0 (no preference) (asterisks at the bottom of the graph denote the significance for these), and Wilcoxon rank sum test with continuity correction for comparing the distributions to each other (n.s.). n=24, n=27.
(C) Egg-laying two-choice preference indices (PI) to yeast odour. One-sample t-test was used to compare the PI to 0. n=10.
(D) Trap assay preference indices (PI) to geosmin for mated and virgin females. Two sample t-test was used for comparing the distributions to each other. n=15 for both groups.
(E) Trap assay choice indices (the % of flies in both traps) for mated and virgin females. Two sample t-test was used for comparing the distributions to each other. n=15 for both groups.
(F) Male courtship indices under geosmin and solvent exposure. Wilcoxon rank sum test with continuity correction for comparing the distributions to each other. n=25 (left), n=28 (right).
(G) Latency to first mating in couples of wild type females with anosmic males under geosmin (right) and solvent (left) exposure. Wilcoxon rank sum test with continuity correction for comparing the distributions to each other. n=52 (left), n=47 (right).
(H) Matings per couple of wild type females with anosmic males during a 23 hour period under geosmin (right) and solvent (left) exposure. Wilcoxon rank sum test with continuity correction for comparing the distributions to each other. n=52 (left), n=47 (right).
(I) Time of matings of wild type females with anosmic males during a 23 hour period (from 0 to 1380 minutes) under geosmin (right) and solvent (left) exposure. Wilcoxon rank sum test with continuity correction for comparing the distributions to each other. n=99 (left), n=93 (right), in 52 and 47 couples, respectively.
(J) A high-resolution close-up of the antennal lobe expression pattern of Or56a-GAL4;R85E04. A maximum intensity projection of a female brain. Green channels marks the driver line expression pattern (Halo2 tag) and magenta the neuropil (SNAP tag). The arrowheads mark the midline crossing typical of ORN axons (white), and the PN cell bodies (grey).
(K) Egg-laying two-choice preference indices (PI) to geosmin while silencing the MB KCs by expressing tetanus toxin light-chain (TNT) [30] via MB247-GAL4. Wilcoxon signed rank test with continuity correction was used for testing the distribution against 0. n=19.

Significance values: * $p<0.05$ ** $p<0.01$

bioRxiv preprint doi: https://doi.org/10.1101/394403; this version posted August 26, 2018. The copyright holder for this preprint (which was not certified by peer review) is the author/funder, who has granted bioRxiv a license to display the preprint in perpetuity. It is made available under aCC-BY-NC 4.0 International license.

Figure S2: Supplementary data 2

(A) An example of a synapse in the FAFB whole-brain EM volume. A DA2 PN is highlighted in green, with the presynapse visible, synaptic cleft in yellow, and the profiles of 7 different postsynaptic neurons in red.
(B) A connectivity diagram of axo-axonic PN synapses between DA2 PNs and to the DL4 PN on the left side of the brain.
(C) Observed versus estimated potential synapses from DA2 PNs to other nearby PNs.
(D) The completion curve for the random sampling from the DA2 PN. Top x axis shows the % of synapses sampled (of all identified synapses in the neuron), bottom x axis the number. Black line represents the number of identified postsynaptic partners (neuron fragments that could not be traced to a soma are excluded) as a function of the number of synaptic connections sampled. Grey line is x=y.
(E) Comparison of the number of synaptic connections found, per partner, in the random sampling (x axis groups) and in total, for all 5 DA2 PNs (y axis), including both fully traced out (cyan) and incomplete neurons (red) in the LH. The dotted lines mark the boundaries for weakly connected (grey line, <5 synapses in total) and very strongly connected (black line, >20 synapses in total) neurons.
(F) The top NBLAST match (red) for Lazarus from the FlyCircuit database.
(G) An example showing dense core vesicles in Lazarus.

Figure S3: Time course of optogenetic behavioural phenotypes and NBLAST matching of AV1a1's to a driver line

(A) The mean PI (to Q1+Q4) as a function of time for LH728, LH1983, Empty-Split GAL4 (genetic control), and Gr66a-GAL4 (a positive aversive control) in the optogenetic behavioural assay. The red squares mark the stimulation epochs. n=16 for all genotypes.
(B) The mean PI and SEM of LH728 plotted against the control line.
(C) The mean PI and SEM of LH1983 plotted against the control line.
(D) A histogram of NBLAST scores of the light-level AV1a1 tracing (from LH1983) to all the EM neurons in the AV1 tract. The primary neurite tract was excluded from the comparisons. AV1a1 Duck (green) and AV1a1 Pigeon (magenta) are indicated.

Figure S4: Downstream sampling curves for PV6a3 Caligari and AV1a1 Duck

(A) The completion curve for the random sampling from PV6a3 Caligari. Top x axis shows the % of synapses sampled (of all identified synapses in the neuron), bottom x axis the number. Black line represents the number of identified postsynaptic partners (neuron fragments without a soma are excluded) as a function of the number of synaptic connections sampled, red line shows an exponential fit for it, and grey line is x=y.
(B) The completion curve for the random sampling from the AV1a1 Duck. Top x axis shows the % of synapses sampled (of all identified synapses in the neuron), bottom x axis the number. Black line represents the number of identified postsynaptic partners (neuron fragments without a

bioRxiv preprint doi: https://doi.org/10.1101/394403; this version posted August 26, 2018. The copyright holder for this preprint (which was not certified by peer review) is the author/funder, who has granted bioRxiv a license to display the preprint in perpetuity. It is made available under aCC-BY-NC 4.0 International license.

soma are excluded) as a function of the number of synaptic connections sampled, red line shows an exponential fit for it, and grey line is x=y.

Figure S1

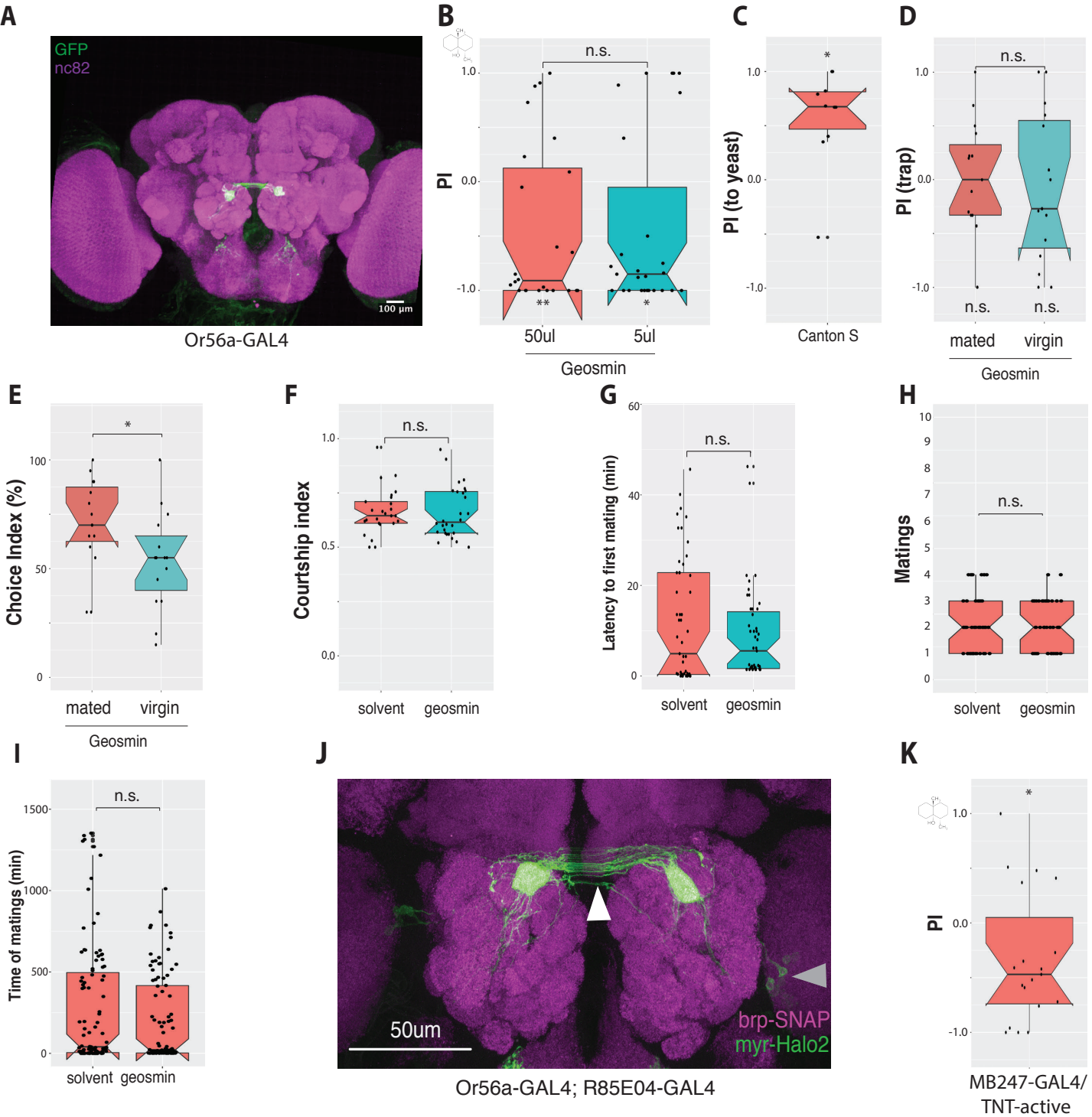
A
GFP
nc82
100 µm
Or56a-GAL4
B
n.s.
PI
1.0
0.0
-1.0
**
*
50ul
5ul
Geosmin
C
*
PI (to yeast)
1.0
0.0
-1.0
Canton S
D
n.s.
PI (trap)
1.0
0.0
-1.0
n.s.
n.s.
mated
virgin
Geosmin
E
*
Choice Index (%)
100
50
0
mated
virgin
Geosmin
F
n.s.
Courtship index
1.0
0.5
0.0
solvent
geosmin
G
n.s.
Latency to first mating (min)
60
40
20
0
solvent
geosmin
H
n.s.
Matings
10
9
8
7
6
5
4
3
2
1
0
solvent
geosmin
I
n.s.
Time of matings (min)
1500
1000
500
0
solvent
geosmin
J
50um
brp-SNAP
myr-Halo2
Or56a-GAL4; R85E04-GAL4
K
*
PI
1.0
0.0
-1.0
MB247-GAL4/
TNT-active

Figure S2

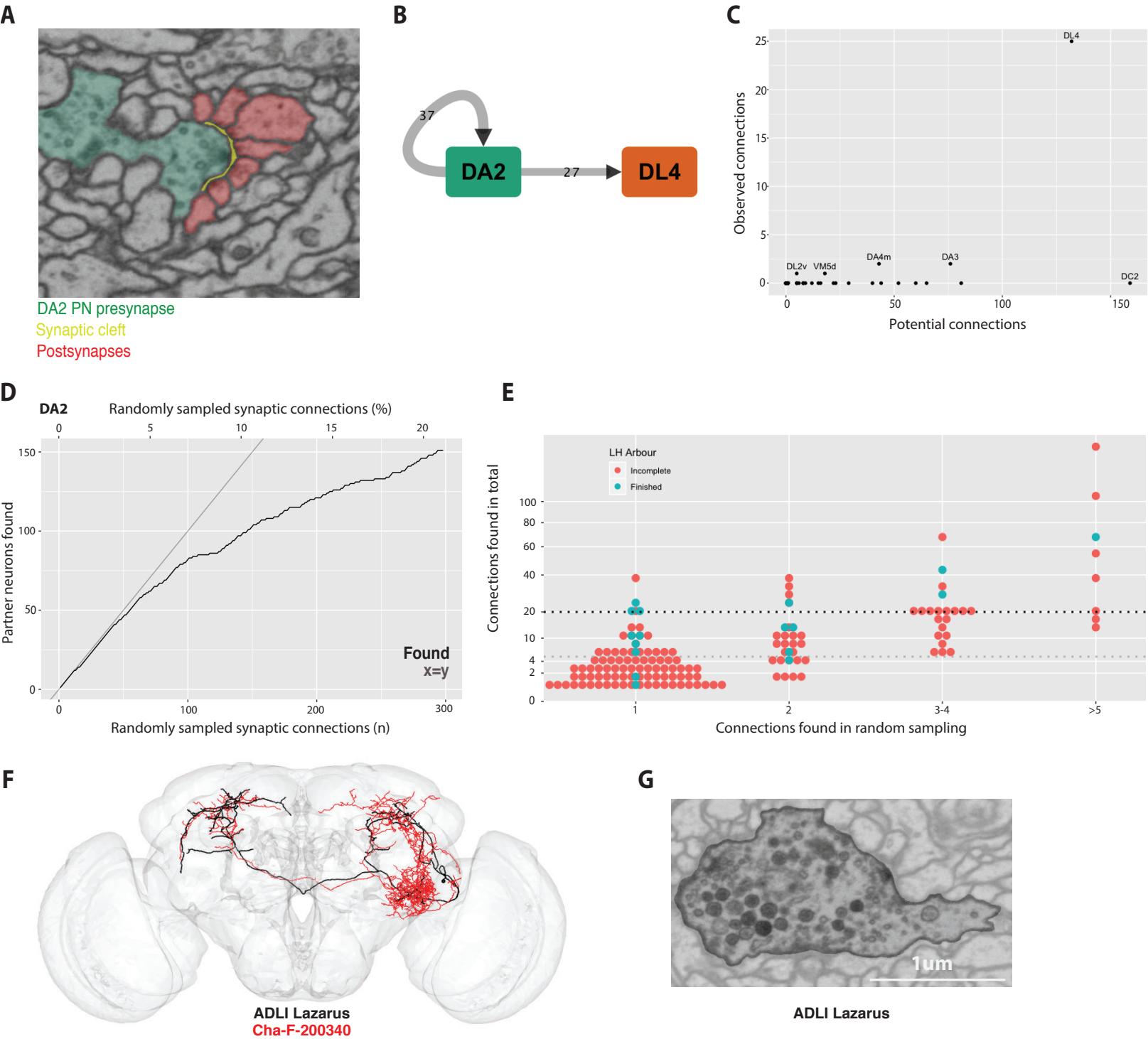
A
DA2 PN presynapse
Synaptic cleft
Postsynapses
B
37
DA2
27
DL4
C
Observed connections
Potential connections
DL4
DA4m
DA3
DL2v
VM5d
DC2
D
DA2
Randomly sampled synaptic connections (%)
Partner neurons found
Randomly sampled synaptic connections (n)
Found
x=y
E
LH Arbour
Incomplete
Finished
Connections found in total
Connections found in random sampling
F
ADLI Lazarus
Cha-F-200340
G
1um
ADLI Lazarus

Figure S3

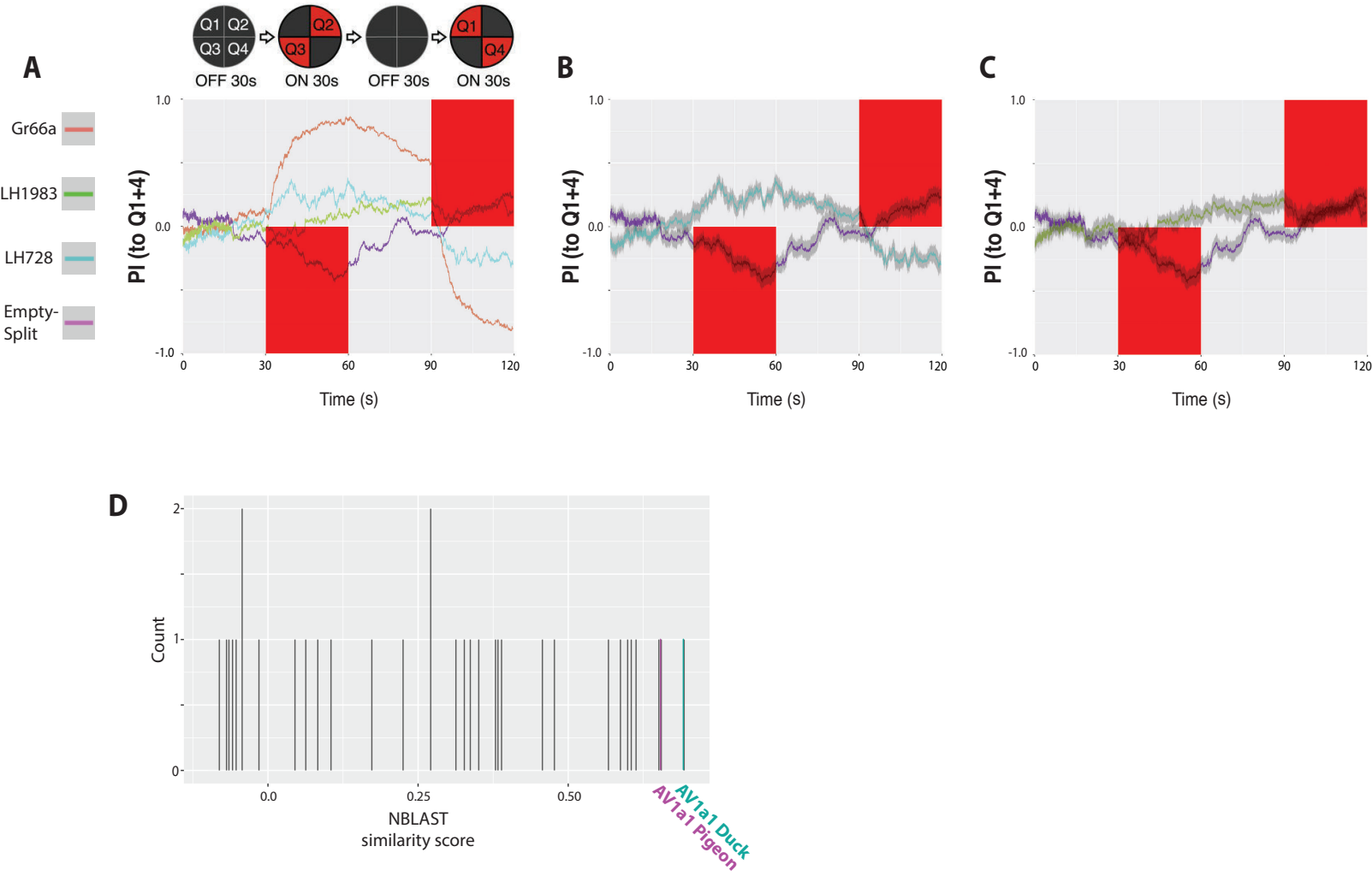
A
Q1 Q2
Q3 Q4
OFF 30s
Q2
Q3
ON 30s
OFF 30s
Q1
Q4
ON 30s
Gr66a
LH1983
LH728
Empty-Split
PI (to Q1+4)
1.0
0.0
-1.0
0
30
60
90
120
Time (s)
B
C
D
Count
2
1
0
0.0
0.25
0.50
NBLAST similarity score
AV1a1 Duck
AV1a1 Pigeon

Figure S4

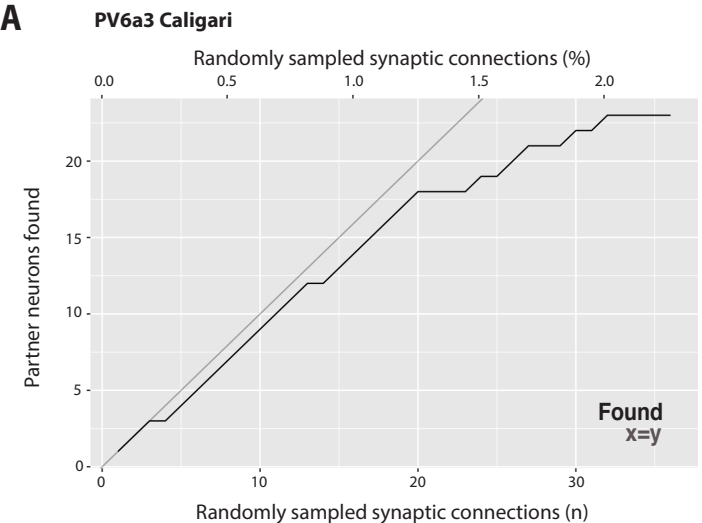
A
PV6a3 Caligari
Randomly sampled synaptic connections (%)
0.0
0.5
1.0
1.5
2.0
Partner neurons found
0
5
10
15
20
0
10
20
30
Randomly sampled synaptic connections (n)
Found
x=y

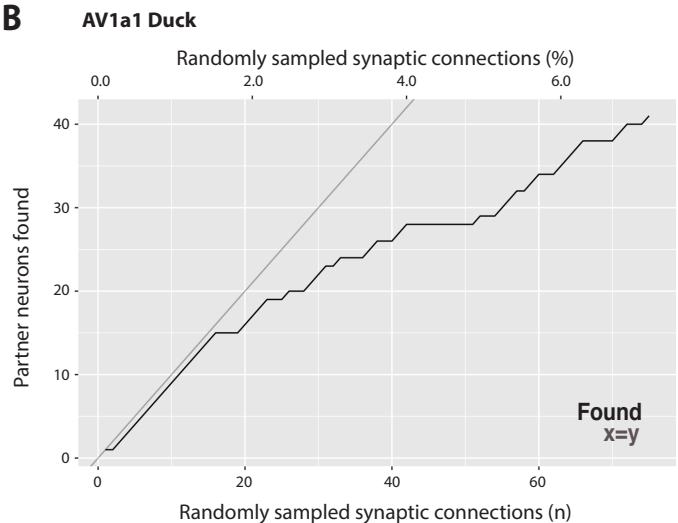
B
AV1a1 Duck
Randomly sampled synaptic connections (%)
0.0
2.0
4.0
6.0
Partner neurons found
0
10
20
30
40
0
20
40
60
Randomly sampled synaptic connections (n)
Found
x=y